Atmos. Chem. Phys., 21, 4575–4597, 2021
https://doi.org/10.5194/acp-21-4575-2021

Atmospheric Chemistry and Physics
Open Access
EGU

Turbulence-permitting air pollution simulation for the Stuttgart metropolitan area

Thomas Schwitalla[1], **Hans-Stefan Bauer**[1], **Kirsten Warrach-Sagi**[1], **Thomas Bönisch**[2], **and Volker Wulfmeyer**[1]

[1]Institute of Physics and Meteorology, University of Hohenheim, Garbenstrasse 30, 70599 Stuttgart, Germany
[2]High-Performance Computing Center Stuttgart (HLRS), Nobelstrasse 19, 70569 Stuttgart, Germany

Correspondence: Thomas Schwitalla (thomas.schwitalla@uni-hohenheim.de)

Received: 16 September 2020 – Discussion started: 30 October 2020
Revised: 3 February 2021 – Accepted: 22 February 2021 – Published: 24 March 2021

Abstract. Air pollution is one of the major challenges in urban areas. It can have a major impact on human health and society and is currently a subject of several litigations in European courts. Information on the level of air pollution is based on near-surface measurements, which are often irregularly distributed along the main traffic roads and provide almost no information about the residential areas and office districts in the cities. To further enhance the process understanding and give scientific support to decision makers, we developed a prototype for an air quality forecasting system (AQFS) within the EU demonstration project "Open Forecast".

For AQFS, the Weather Research and Forecasting model together with its coupled chemistry component (WRF-Chem) is applied for the Stuttgart metropolitan area in Germany. Three model domains from 1.25 km down to a turbulence-permitting resolution of 50 m were used, and a single-layer urban canopy model was active in all domains. As a demonstration case study, 21 January 2019 was selected, which was a heavily polluted day with observed PM_{10} concentrations exceeding $50\,\mu g\,m^{-3}$.

Our results show that the model is able to reasonably simulate the diurnal cycle of surface fluxes and 2 m temperatures as well as evolution of the stable and shallow boundary layer typically occurring in wintertime in Stuttgart. The simulated fields of particulates with a diameter of less than 10 µm (PM_{10}) and nitrogen dioxide (NO_2) allow a clear statement about the most heavily polluted areas apart from the irregularly distributed measurement sites. Together with information about the vertical distribution of PM_{10} and NO_2 from the model, AQFS will serve as a valuable tool for air quality forecasting and has the potential of being applied to other cities around the world.

1 Introduction

Currently, more than 50 % of the global population lives in cities, whereas the United Nations (UN) expect a further increase by about 10 % in 2030 (UN, 2018). The UN also expects that in 2030 34 % of the world population will reside in cities with more than 500 000 inhabitants.

Due to a strong increase of road traffic in major European cities (Thunis et al., 2017), pollution limits are often violated in larger cities. For example, for particulate matter with particle diameters less than 10 µm (PM_{10}), the critical value is an annual mean concentration of $20\,\mu g\,m^{-3}$ or a daily mean value of $50\,\mu g\,m^{-3}$ (WHO, 2005). For nitrogen dioxide (NO_2), the critical values are 200 and $40\,\mu g\,m^{-3}$ as daily and annual mean values, respectively.

The violation of these pollution limits can lead to health and environmental problems and is currently part of several litigations, e.g., at the German Federal Administrative Court dealing with possible driving bans for non-low-emission vehicles. The basis for these litigations are mostly a few local, unevenly distributed observations. In combination with special meteorological conditions like wintertime thermal inversion layers, it can be misleading to draw conclusions about the overall air quality in the city only from single observations. According to, e.g., the German Federal Immission Control Ordinance (https://www.gesetze-im-internet.de/bimschv_39/anlage_3.html, last access: 23 March 2021), it is sufficient that traffic-related measurements are representative of a section of 100 m, but this is not representative of the commercial and office districts in the cities that are suffering from traffic control in the case of fine dust alerts and residential areas. Namely in residential areas, health protection action plans require representative air quality measures.

Therefore, it becomes important to apply a more scientifically valid approach by applying coupled atmospheric and chemistry models to predict air quality. Regional and global atmospheric models like the Weather Research and Forecasting (WRF) model (Skamarock et al., 2019), the Consortium for Small Scale modeling (COSMO; Baldauf et al., 2011), the Icosahedral Nonhydrostatic model (ICON; Zängl et al., 2015), or the Regional Climate Model system (RegCM4; Giorgi et al., 2012) are often used to force offline chemistry transport models like CHIMERE (Mailler et al., 2017), LOng Term Ozone Simulation – EURopean Operational Smog (LOTOS-EUROS) (Manders et al., 2017), EURopean Air Pollution Dispersion (EURAD; Memmesheimer et al., 2004), and Model for OZone And Related chemical Tracers (MOZART) (Brasseur et al., 1998; Horowitz et al., 2003).

Several studies showed that combining an atmospheric model with an online coupled chemistry component is a suitable tool for air quality and pollution modeling in urban areas at the convection-permitting (CP) resolution (Fallmann et al., 2014; Kuik et al., 2016, 2018; Zhong et al., 2016; Huszar et al., 2020) .

Compared to chemical transport models, coupled models like the Weather Research and Forecasting model with its coupled chemistry component (WRF-Chem) (Grell et al., 2005), COSMO-ART (Vogel et al., 2009), ICON-ART (Rieger et al., 2015), and the Integrated Forecasting System (IFS) MOZART (Flemming et al., 2015) allow for a direct interaction of aerosols with radiation, leading to a better representation of the energy balance closure at the surface as would be the case when applying an offline chemistry model.

As the terrain and land cover over urban areas usually show fine-scale structures which are not resolved even by a CP resolution, there is a need for turbulence-permitting (TP) simulations with horizontal grid increments of a few hundred meters or even less. Important features are, e.g., urban heat island effects (Fallmann et al., 2014, 2016; García-Díez et al., 2016; Li et al., 2019) and local wind systems like mountain and valley winds due to differential heating (Corsmeier et al., 2011; e.g., Jin et al., 2016). Also, micro- and mesoscale wind systems can develop due to urban structures and the heterogeneity of the land surface. It is well known that TP simulations are a promising tool to further enhance the understanding of processes in the atmospheric boundary layer (Heinze et al., 2017a, b; Panosetti et al., 2016; Bauer et al., 2020) in urban areas (Nakayama et al., 2012; Maronga et al., 2019, 2020).

In order to further enhance the quality of the simulations, building and urban canopy models (UCMs) are developed (Martilli et al., 2002; Kusaka and Kimura, 2004; Salamanca and Martilli, 2010; Maronga et al., 2019; Scherer et al., 2019; Teixeira et al., 2019). The main purpose of UCMs is to provide a better description of the lower boundaries over urban areas such as building, roof, and road geometries and their interactions with atmospheric water vapor, wind, and radiation.

With the EU-funded "Open Forecast" project (https://open-forecast.eu/en/, last access: 23 March 2021), it was intended to develop a prototype for an air quality forecasting system (AQFS) for the Stuttgart metropolitan area in southwest Germany. Open Forecast is a demonstration project to show the potential of open data combined with supercomputer resources to create new data products for European citizens and public authorities. The long-term goal is to provide end users and political decision makers a useful tool, particularly considering further urbanization and heat island effects as well as potential driving restrictions due to recent EU decisions on emission limits.

For our AQFS, we use the WRF-Chem NWP model (Grell et al., 2005; Skamarock et al., 2019), as the WRF model is extensively evaluated over Europe at different timescales and horizontal resolutions (San José et al., 2013; Warrach-Sagi et al., 2013; Milovac et al., 2016; Lian et al., 2018; Molnár et al., 2019; Bauer et al., 2020; Coppola et al., 2020; Schwitalla et al., 2020). It can easily be set up in a nested configuration over all regions of the Earth. Compared to the Parallelized Large-Eddy Simulation Model (PALM) (Maronga et al., 2015) for urban applications (PALM-4U), the nested model domains are driven by the full atmospheric and chemical information from the parent domain along its lateral boundaries. Also, it contains well-characterized combinations of parameterizations of turbulence and cloud microphysics in the outer domain that are consistent with the inner TP domains where the high-quality cloud parameterization remains. No switch between different model systems is required, which is expected to provide a great advantage with respect to the skill of air pollution and meteorological forecasts.

To enhance the forecast skill, suitable variational and ensemble-based data assimilation systems are already in place to further improve the meteorological initial conditions (Barker et al., 2012; Zhang et al., 2014; Kawabata et al., 2018; Thundathil et al., 2020) and the chemical initial conditions (Chen et al., 2019; Sun et al., 2020), but this is beyond the scope of our study.

The PALM model is another widely used TP simulation model over Europe. PALM did not include the full interaction between land surface, radiation, cloud microphysics, and chemistry during the performance of our study. The very recent version (6.0) of PALM-4U (Maronga et al., 2020) is expected to contain a fully coupled chemistry module (Khan et al., 2021).

Fallmann et al. (2016) and Kuik et al. (2016) performed air quality simulations with WRF-Chem over the cities of Berlin and Stuttgart on a CP resolution down to 1 km and less than 40 model levels. They used the Netherlands Organ-

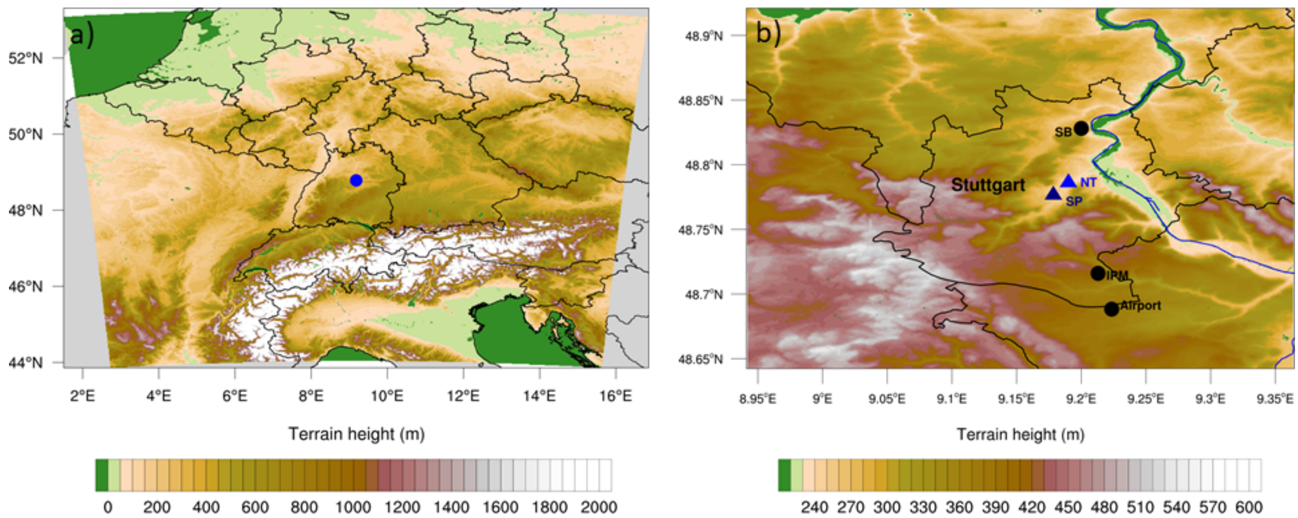

Figure 1. Model domain 1 **(a)** and domain 3 **(b)**. The blue dot in panel **(a)** denotes Stuttgart. Black dots in panel **(b)** show the location of the meteorological measurement sites. The diamonds in panel **(b)** denotes the Neckartor (NT) and Schlossplatz (SP) locations and the blue contour line denotes the Neckar River (river data © OpenStreetMap contributors 2020. Distributed under a Creative Commons BY-SA License).

isation for Applied Scientific Research – Monitoring Atmospheric Composition and Climate (TNO-MACC) emission inventory (Kuenen et al., 2014), which is available as an annual total on a 7 km × 7 km resolution. As the topography of Stuttgart is very complex, the AQFS applies the WRF-Chem model on a TP horizontal resolution using 100 model levels to account for the shallow boundary layer occurring during wintertime. In addition, we applied a local emission data set from the Baden-Württemberg State Institute for the Environment, Survey and Nature Conservation available as annual mean on a horizontal resolution of 500 m × 500 m to resolve fine-scale emission structures.

Our study focuses on the methodology how to set up a AQFS prototype by using WRF-Chem and its application to a typical wintertime situation during January 2019 in the Stuttgart metropolitan area. The paper is set up as follows: Sect. 2 describes the design of our AQFS model system on the TP resolution of 50 m, followed by a description of the selected case study. Section 4 shows the results with respect to meteorological variables and air quality including a discussion. Section 5 summarizes our work and provides an outlook on potential future enhancements of the AQFS prototype.

2 AQFS design

2.1 WRF model setup

For our AQFS prototype, we selected the Advanced Research WRF-Chem model version 4.0.3 (Grell et al., 2005; Skamarock et al., 2019). To reach the targeted resolution of 50 m, three model domains have been applied, with horizontal resolutions of 1250, 250, and 50 m, and encompass 800 × 800 grid cells in the outer domain and 601 × 601 grid cells in the two inner TP domains. The reasons for starting with a resolution of 1250 m in the outermost domain are (1) to avoid the application of a convection parametrization which can deteriorate the model results (Prein et al., 2015; Coppola et al., 2020), (2) so that the model starts to partially resolve turbulent structures, whilst a planetary boundary layer (PBL) parametrization is still necessary (Honnert and Masson, 2014; Honnert et al., 2020), and (3) to reach the target resolution with a nesting ratio of 5 : 1. The areas of model domains 1 and 3 are shown in Fig. 1.

As seen from Fig. 1b, the Stuttgart metropolitan area is characterized by an elevation variation of more than 300 m. The lowest elevation is approximately 220 m in the basin, while the highest elevation reaches up to 570 m. As the main traffic roads are in the basin, especially during wintertime, this often leads to a worsening of the air quality as the surrounding prevents an air mass exchange due to the stationary temperature inversion.

For the WRF model system, land cover and soil texture fields are not available at resolutions higher than 500 m. Therefore, we reclassified land cover data from the Copernicus Coordination of Information on the Environment (CORINE) Land Cover (CLC) 2012 data set (European Union, 2012), available on a resolution of 100 m, from the original 44 categories to the categories applied in the WRF model for the simulations of the outer two domains. For the innermost model domain, we incorporated the most recent high-resolution land cover data set from the Baden-Württemberg State Institute for the Environment (LUBW), which was derived from Landsat (Butcher et al., 2019) in 2010 and is available at 30 m resolution (https://udo.lubw.

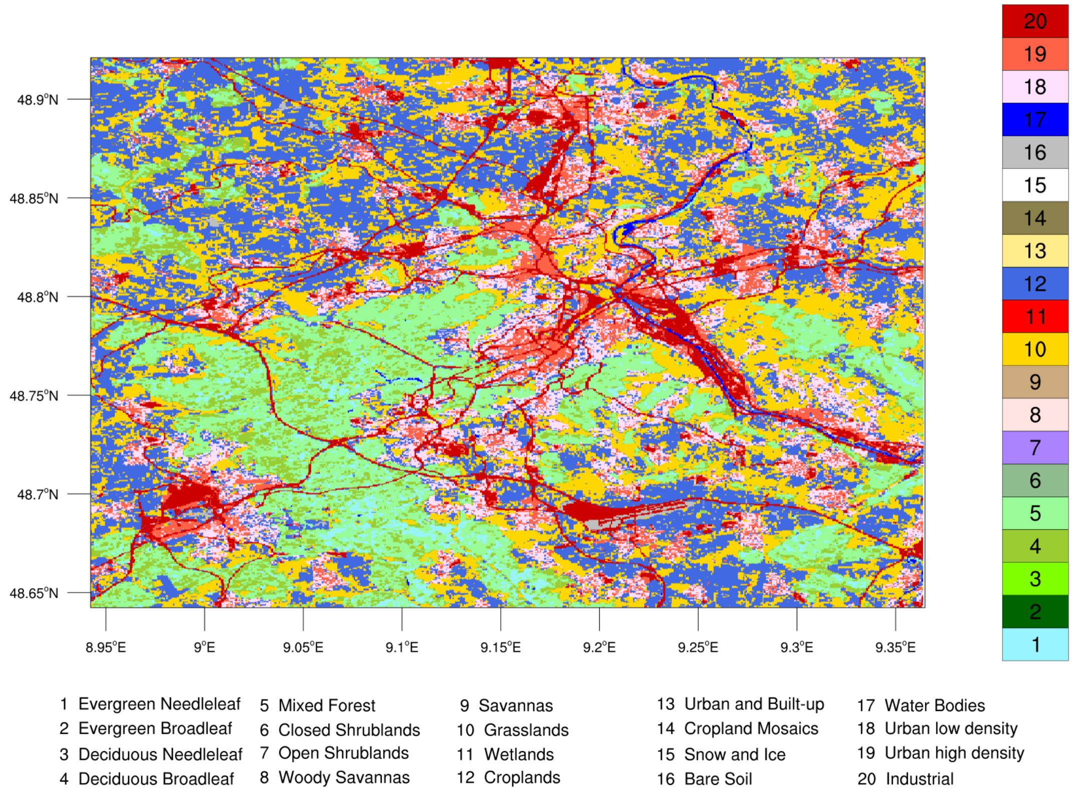

Figure 2. Land cover data from the Baden-Württemberg State Institute for the Environment (LUBW) reclassified for WRF in the innermost domain at a resolution of 50 m.

baden-wuerttemberg.de/public/, last access: 23 March 2021). This data set was also reclassified to the corresponding land cover categories used in WRF and is shown in Fig. 2.

The resolution of the provided default Food and Agriculture Organization of the United Nations (FAO) soil texture data is only 10 km; therefore, we used soil texture data from the International Soil Reference and Information Centre (ISRIC) SoilGrids project (Hengl et al., 2014, 2015). These data are available on a resolution of 250 m. Terrain information was provided by the National Center for Atmospheric Research (NCAR) derived from the global multi-resolution terrain elevation data 2010 (GMTED2010) data set (Danielson and Gesch, 2011) for domain 1. As the horizontal resolution of the GMTED2010 data set is 1 km, the 3 arcsec gap-filled Shuttle Radar Topography Mission (SRTM) data set (Farr et al., 2007) is used for domain 2. As this resolution is still too coarse for our targeted resolution of 50 m, the European Union digital elevation model (EU-DEM; European Union, 2017), available at a resolution of 25 m, is used for the innermost domain.

In our setup, we use 100 vertical levels for all domains using the traditional terrain following coordinate system in WRF; 20 of the levels are distributed in the lowest 1100 m a.g.l. (above ground level). All domains apply the Noah-MP land surface model (Niu et al., 2011; Yang et al., 2011), the revised MM5 (Fifth-Generation Penn State/NCAR Mesoscale Model) surface layer scheme based on Monin–Obukhov similarity theory (Jiménez et al., 2012), the Thompson two-moment cloud microphysics scheme (Thompson et al., 2008), and the Rapid Radiative Transfer Model for GCMs (RRTMG; Iacono et al., 2008) for parametrizing longwave and shortwave radiation. Due to the coarser resolution of the outermost domain, we applied the Yonsei University (YSU; Hong et al., 2006) PBL parametrization in D01 only. As suggested by the WRF user guide, we applied the subgrid turbulent stress option for momentum (Kosovic, 1997) in domains 2 and 3. The complete namelist settings are provided in the Supplement.

The more sophisticated building effect parameterization (BEP; Martilli et al., 2002) is not applied, as this scheme does not work with our selection of parameterizations. Instead, the single-layer urban canopy model (UCM) (Kusaka and Kimura, 2004) is selected to improve the representation of the urban canopy layer and the surface fluxes. The parameters needed by the UCM are read in from the lookup table (URBPARAM.TBL), which was adjusted for the Stuttgart area following Fallmann (2014).

Atmospheric chemistry is parameterized by the Regional Acid Deposition Model second generation (RADM2) model (Stockwell et al., 1990). RADM2 features more than

60 chemical species and more than 135 chemical reactions including photolysis. Aerosols are represented by the Modal Aerosol Dynamics Model for Europe (MADE) and Secondary Organic Aerosol Model (SORGAM) scheme (Ackermann et al., 1998; Schell et al., 2001) considering size distributions, nucleation, coagulation, and condensational growth. The combination of RADM2–MADE–SORGAM is a computationally efficient approach and is widely used for simulations over Europe (Forkel et al., 2015; Mar et al., 2016). To further enhance vertical mixing of CO to higher altitudes during nighttime over urban grid cells, the "if" statements in the dry deposition driver of WRF-Chem at lines 690 and 707 have been deleted accordingly, as shown in the Supplement of Kuik et al. (2018).

Compared to a previous study from Fallmann et al. (2016), who performed simulations over the Stuttgart metropolitan area using WRF-Chem on a CP resolution of 3 km, or the study of Kuik et al. (2016), who performed a 3-month simulation at different resolutions over Berlin, simulations on the TP resolution provide a much more realistic representation of the land cover structures (see Fig. 2 in this paper and, e.g., Fig. 2b in Fallmann et al., 2016). As the climate in the Stuttgart metropolitan area is strongly influenced by the topography, we are convinced that our special combination of a TP resolution and high-resolution emission data (see Sect. 2.3) will lead to a better understanding and prediction of the air pollution situation in this area.

Currently, air pollution modeling with WRF-Chem is a computationally expensive task. Depending on the number of output variables and frequency (5 min in our study), a 24 h simulation currently takes around 36 h wall-clock time. For future experiments, it is worth trying the I/O quilting option in combination with PnetCDF, which should considerably reduce the time spent on I/O.

While the WRF model itself is ready for hybrid parallelism (MPI plus OpenMP), the WRF-Chem model can only be used with MPI. If WRF-Chem could be enhanced for additional OpenMP capabilities, this would lead to an increase in computation speed that is almost linear with the number of OpenMP threads.

Due to the complexity of the chemistry model in combination with the very high horizontal resolution and the calm meteorological conditions, the adaptive model time step option was chosen instead of a fixed time step. Model output is available in 5 min intervals for the innermost model domain.

Our single-day case study on the TP scale is designed to serve as a test bed to set up an air quality forecasting system prototype for the Stuttgart metropolitan area. For process studies, the model chain itself can be applied to other areas over the globe as long as (1) detailed land cover and soil texture data are available and (2) high-resolution emission data not only from traffic are available. The new model system can be even applied in a forecast and warning mode if near-real-time emissions as well as meteorological and chemical input data are available in a timely manner. As the computational demands of applying WRF-Chem on the TP scale are very high, access to an high-performance computing (HPC) system is a prerequisite.

2.2 Model initialization

The meteorological initial and boundary conditions were provided by the operational ECMWF integrated forecasting system (IFS) analysis on model levels. The IFS is a global model with 9 km horizontal resolution and applies a sophisticated four-dimensional variational (4D-Var) data assimilation system (Bonavita et al., 2016). The data have been retrieved from the ECMWF Meteorological Archival and Retrieval System (MARS) and were interpolated to a resolution of 0.05°.

The initialization and provision of the boundary conditions of the chemistry of the model are done with data from the Whole Atmosphere Community Climate Model (WACCM; Marsh et al., 2013) using MOZART conversion tool (MOZBC) (Pfister et al., 2011). As the resolution of WACCM is very coarse, the input data were enhanced by the ECMWF Copernicus Atmosphere Monitoring Service (CAMS) reanalysis data set on 60 model levels and 40 km horizontal resolution (Inness et al., 2019).

2.3 Emission data

The emission data set used in this study is a combination of three products. Global input data sets containing coarse resolution emissions from different sources are obtained from the Brazilian developments on the Regional Atmospheric Modeling System (BRAMS) numerical modeling system (Freitas et al., 2017). The PREP-CHEM-SRC tool (Freitas et al., 2011) is then applied as pre-processor to convert these emissions to the appropriate WRF units and interpolate the data onto the WRF model grid.

As global emission data sets have a very coarse resolution in space and time, higher-resolution emission data for Europe from the CAMS-REG-AP product (Copernicus Atmosphere Monitoring Service – CAMS; Copernicus, 2020) became available (Granier et al., 2019). Its resolution is approximately 7 km × 7 km, and it is based on total annual emissions from 2016. This product provides emissions of PM_{10}, $PM_{2.5}$, SO_2, CO, NO_x, and CH_4 and contains sources from different sectors, separated into 10 different categories following the Gridded Nomenclature For Reporting (GNFR; Granier et al., 2019).

The third emission data set (BW-EMISS) deployed in our study was obtained from the LUBW. This data set contains annual mean emissions from different sectors following the GNFR classification, and it is currently available only until 2014 and has a horizontal resolution of 500 m. Unfortunately, more recent quality-controlled data sets were not available when our study was performed. It is expected that annual emissions for 2018 will become available by mid-2021.

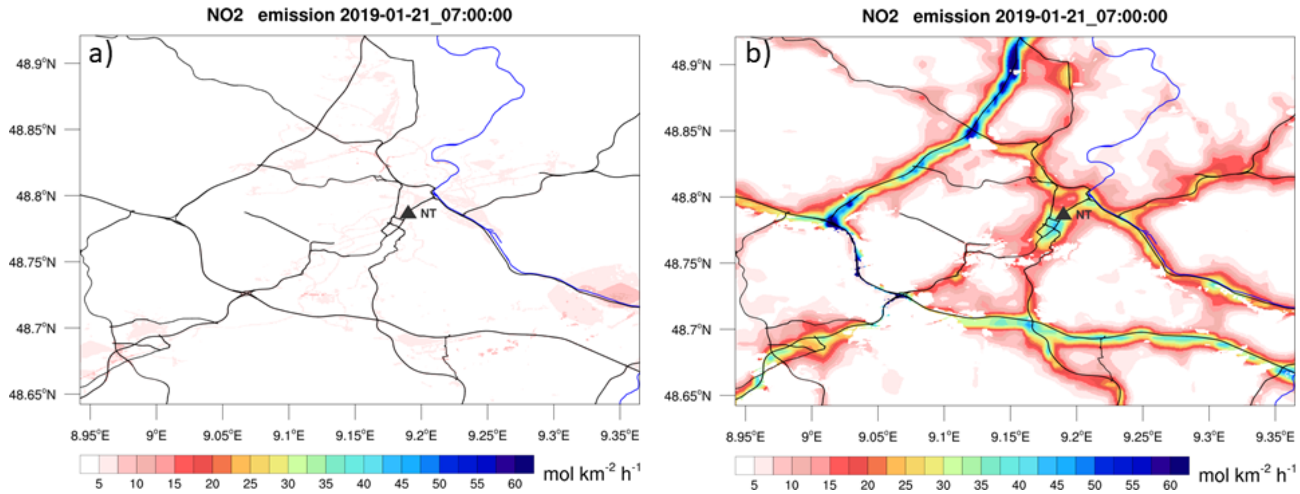

Figure 3. NO_2 emissions valid at 07:00 UTC on 21 January 2019. Panel **(a)** shows the emissions derived from the CAMS-REG-AP data set and **(b)** shows the emissions derived from the BW-EMISS data set (map data © OpenStreetMap contributors 2020. Distributed under a Creative Commons BY-SA License).

As CAMS-REG-AP and BW-EMISS only contain annual sums or annual mean values, a temporal decomposition was applied for both data sets following Denier van der Gon et al. (2011). Depending on the GNFR code, the data are first projected onto the corresponding month, followed by the corresponding day of the week and the hour of the day. A similar approach was performed, e.g., in Resler et al. (2020, under review) for the city of Prague. After finishing the decomposition, the data were converted to the corresponding units and interpolated onto the WRF model grid using the Earth System Modeling Framework (ESMF; Valcke et al., 2012) interpolation utilities.

Figure 3 shows an example of the NO_2 emissions derived from the CAMS-REG-AP product (Fig. 3a) and the emission data derived from the LUBW data set (Fig. 3b) on 21 January 2019 at 07:00 UTC.

Due to its much higher horizontal resolution, the BW-EMISS data set (Fig. 3b) shows much more detailed structures for the NO_2 emissions which are mainly caused by road traffic. The average emissions for this particular time step are 2 $\mathrm{mol\,km^{-2}\,h^{-1}}$ for the CAMS-REG-AP data set and 7 $\mathrm{mol\,km^{-2}\,h^{-1}}$ for the BW-EMISS data set.

In addition, the following adjustments have been performed: (1) NO_x emissions from forest grid cells have been reduced by 90 %, (2) road traffic NO_x emissions were transformed into 90 % NO and 10 % NO_2 emissions following Kuik et al. (2018), (3) all emissions from Stuttgart Airport were reduced by 90 % during the nighttime flight ban between 00:00 and 04:00 UTC as well as after 21:00 UTC.

The WRF-Chem model only ingests one emission data set per species; hence, emissions from the different GNFR categories have accumulated in a single emission data set before performing the simulation. Figure 4 summarizes all necessary steps and the complete data and workflow of the AQFS prototype.

2.4 Observations

We used data from three meteorological stations: Stuttgart-Schnarrenberg (48.8281° N, 9.2° E; elevation 314 m), Stuttgart Airport (48.6883° N, 9.2235° E; elevation 375 m), and the Institute of Physics and Meteorology (IPM) at the University of Hohenheim (48.716° N, 9.213° E; elevation 407 m) to validate the simulated 2 m temperatures; data are available every 10 min. The locations are indicated by the black dots in Fig. 1b. In addition, the radiosonde data from Stuttgart-Schnarrenberg were used.

3 Case study description

For our study, we selected 21 January 2019. This day was characterized as "fine dust alarm" situation (Stuttgart Municipality and German Meteorological Service (DWD), 2019), which is defined by a combination of the following criteria:

1. expected daily maximum PM_{10} concentration at Stuttgart Neckartor (NT in Fig. 1b) is higher than 30 $\mathrm{\mu g\,m^{-3}}$;
2. no rain on the following day;
3. 10 m wind speed less than 3 $\mathrm{m\,s^{-1}}$ from the south to northwest directions (180–330°);
4. nocturnal atmospheric inversion;
5. mixing layer depth less than 500 m during the day;

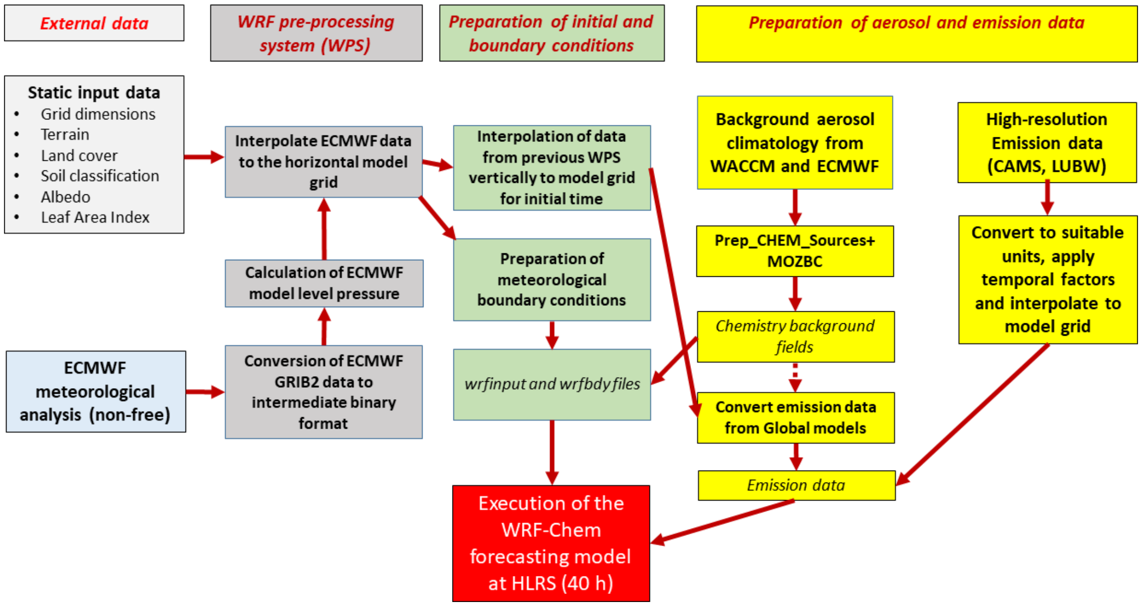

Figure 4. Workflow of the AQFS prototype system.

6. daily average 10 m wind speed less than $3\,m\,s^{-1}$ from all directions.

A sufficient criterion is a higher PM_{10} concentration following (1). If (1) is not fulfilled, then (2) and (3) together with either (4) and/or (5) have to be fulfilled. If only (4) or (5) is fulfilled, then (6) has to be considered. For our case study, criteria (1)–(5) were fulfilled.

The solid lines in Fig. 5 show the observed PM_{10} and NO_2 concentrations at several stations in our model domain. From Fig. 5a, the high NO_2 concentrations at Neckartor and Hohenheimer Strasse occurring after sunrise can be clearly identified. While these measurements are taken next to main roads, the other stations show considerably lower NO_2 concentrations throughout the day. The PM_{10} concentrations (Fig. 5b) show extremely high values at Neckartor, exceeding $100\,\mu g\,m^{-3}$ around noon and the evening rush hour which clearly meets the main criteria of the “fine dust alarm” situation. The other stations, which are not directly located near main roads with heavy traffic, show considerably lower PM_{10} concentrations around $40\,\mu g\,m^{-3}$.

This day was a typical winter weather situation. Central Europe was located at the east flank of a blocking high-pressure system located over the eastern Atlantic together with moderate to low horizontal geopotential gradients and resulting weak winds at 500 hPa in southwestern Germany (Fig. 6a).

Near-surface temperatures are below freezing level, between 1000 and 850 hPa very light easterly winds characterize the flow, and a dry layer is present around 925 hPa (Fig. 6b). Above 850 hPa, the wind direction rapidly changes to westerly directions, but the wind speeds remain below $5\,m\,s^{-1}$ (see Fig. 7a).

The inversion between the two air masses inhibits vertical mixing, leading to higher concentrations of aerosols in the lowest few hundred meters above ground level (AGL) and preventing air mass exchange aloft. This inversion is further enhanced by the special orography of the city of Stuttgart.

4 Results and discussion

4.1 Meteorological quantities

Figure 7a shows a Skew-T diagram of the model initial conditions (black line) at Stuttgart-Schnarrenberg valid at 00:00 UTC on 21 January 2019 in comparison with the observations (red line).

The initial conditions agree well with the sounding showing a weak temperature inversion around 900 hPa with high relative humidity values up to 650 hPa. The observed and simulated lifting condensation level is 940 hPa and the integrated water vapor (PWAT) is 8 mm. Wind speed and direction agree with the observations, showing a wind shear above 850 hPa associated with low wind speeds of less than $5\,m\,s^{-1}$.

To further evaluate the stratification conditions during the day, Fig. 7b shows the observed and simulated temperature, dew point, and wind profiles at 11:00 UTC. The vertical structure of the observation and the simulation has an almost perfect agreement. The temperature inversion layer at 910 hPa is well captured, although the simulated temperatures below the inversion are too high by about 1.5 K. The humidity profile (expressed as a dew-point profile) is also very well captured with the largest moisture content below 870 hPa. Wind speed and direction above 850 hPa agree well

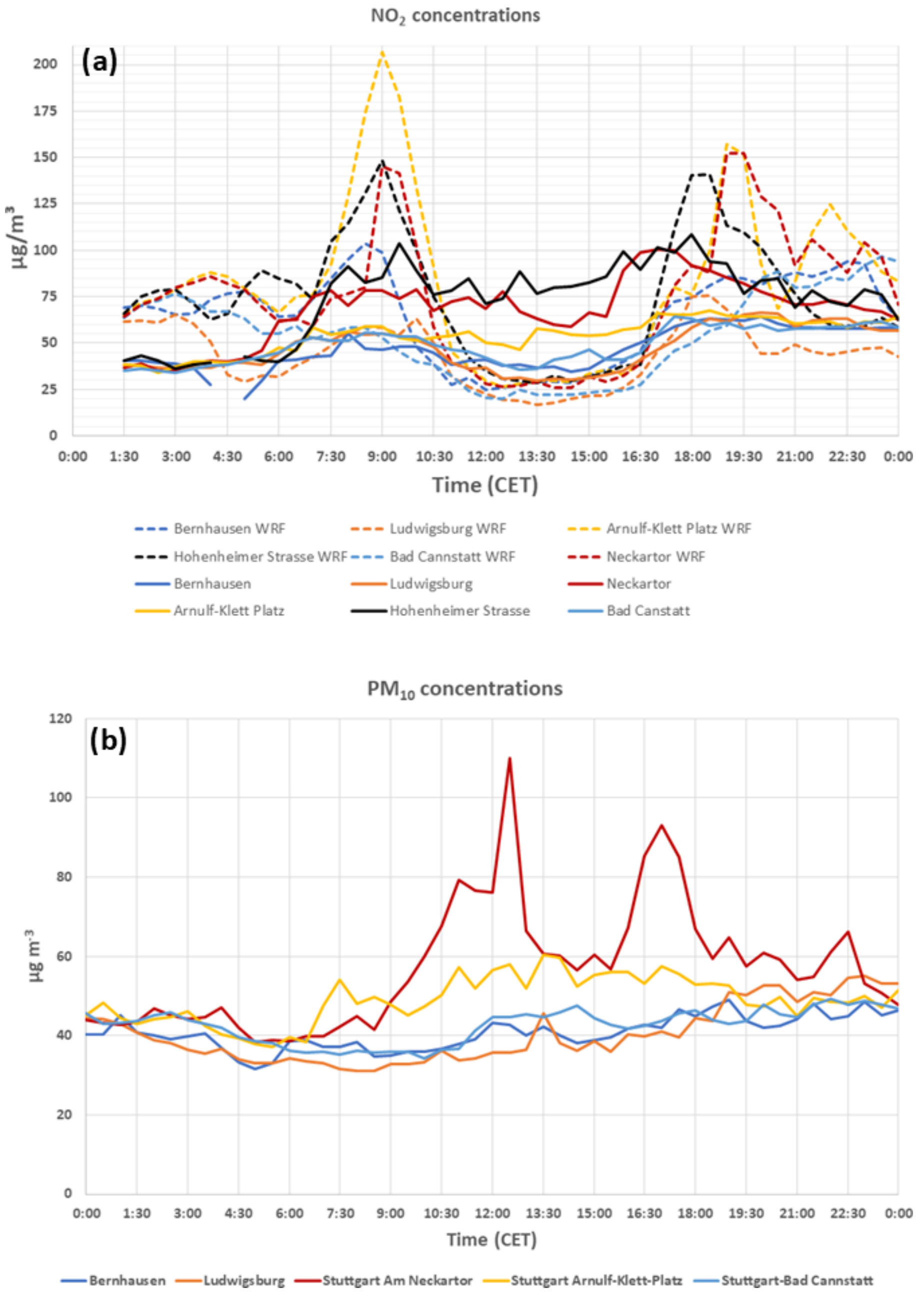

Figure 5. NO_2 **(a)** and PM_{10} **(b)** concentrations at several stations distributed over the model domain on 21 January 2019. The dashed line in panel **(a)** denotes the simulated NO_2 concentration and the time zone (CET) corresponds to local time. Measurements at Neckartor, Hohenheimer Strasse, and Arnulf-Klett Platz are directly taken next to the main road.

with the observation throughout the atmosphere. With regard to the vertical model resolution, the wind situation in the lowest 1000 m a.g.l. is also reasonably represented.

Figure 8 exemplarily shows the simulated 2 m temperature together with 10 m wind velocities at 12:00 UTC (noon) to display the complexity of the Stuttgart metropolitan area.

The 2 m temperatures show a daytime warming of downtown Stuttgart and the Neckar Valley, while temperatures slightly below 0 °C are still present at higher elevations (blue colors in Fig. 8). The wind situation is very complex due to weak wind speeds in combination with a shallow boundary layer (see Fig. 16), but the wind flow along the upper Neckar River (south of 48.75° N) is strongly pronounced. After sunset, wind speed starts to decrease and the channeling effect along the Neckar weakens (not shown).

Figure 9 shows an evaluation of the diurnal cycle of 2 m temperatures at the three measurement sites Schnarrenberg, IPM and airport. Sunrise is at 07:00 UTC and sunset at

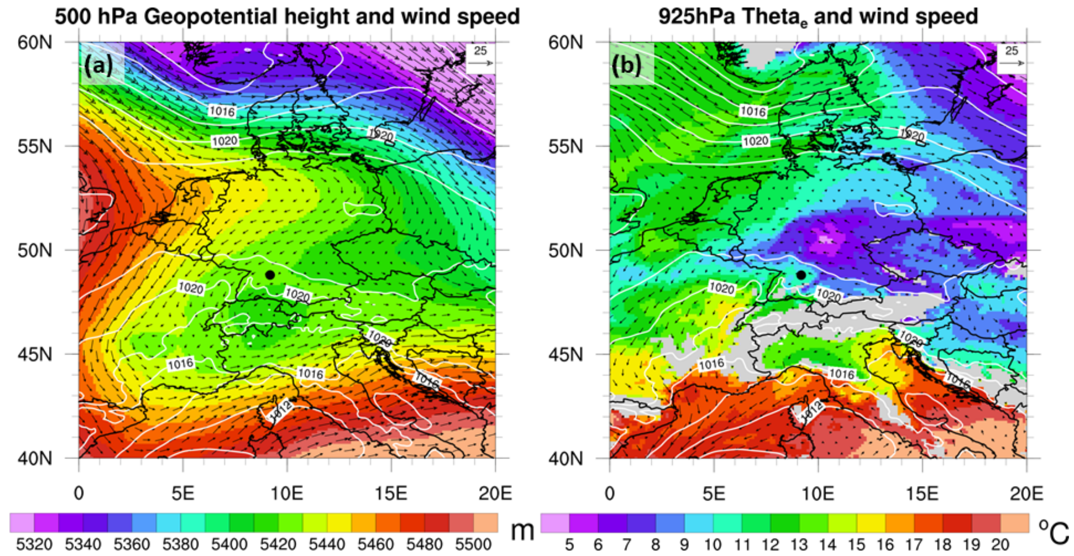

Figure 6. (a) ECMWF operational analysis of 500 hPa geopotential height, sea level pressure (white contour lines) together with 500 hPa wind velocities valid at 00:00 UTC on 21 January 2019. Panel **(b)** shows the 925 hPa equivalent potential temperature together with 925 hPa wind velocities and sea level pressure (white contour lines). Gray areas indicate values below the ECMWF model terrain. The black dot denotes Stuttgart, and the reference wind vector length (top right corner of each figure) is equal to 25 $m s^{-1}$.

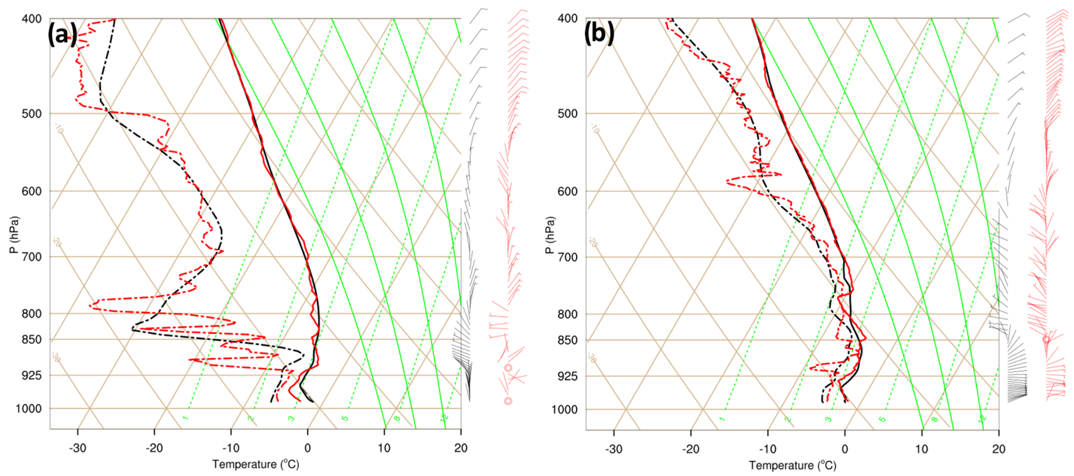

Figure 7. Comparison of temperature, dew-point and wind of the WRF model simulation (black line) and the sounding from Stuttgart-Schnarrenberg (red line) valid at 00:00 UTC **(a)** and 11:00 UTC **(b)** on 21 January 2019. The solid lines denote the temperature profile and the dash-dotted line denotes the dew-point profile. Wind barbs denote wind speed in $m s^{-1}$.

16:00 UTC, and the model data are averaged over five grid cells around the measurement site to take into account that even a simulation with 50 m resolution cannot fully capture the local conditions at the measurement site. The northern station (Schnarrenberg) shows a lower temperature throughout the day than the other two stations, which are situated 3 km apart at a similar elevation. The temperature is about 1 K colder during the day and 0.5 K colder during the night.

At Schnarrenberg, the observed diurnal cycle is reasonably well simulated with WRF. Between 00:00 and 15:00 UTC, a warm temperature bias of 1 K is present in the simulation, which turns into a small negative bias after sunset. At IPM, the simulation shows a cold bias until 04:00 UTC turning into a warm bias as the strong temperature drop is not simulated until 06:30 UTC. After 09:00 UTC until sunset, the simulated temperature agrees well with the observations, while later a cold bias of around 1 K is present.

For the airport station, the model stays too warm with a positive bias of almost 2 K between 05:00 and 09:00 UTC. During the further course of the day, the bias reduces to 1 K at noon, while after sunset it turns into a negative bias of 1 K.

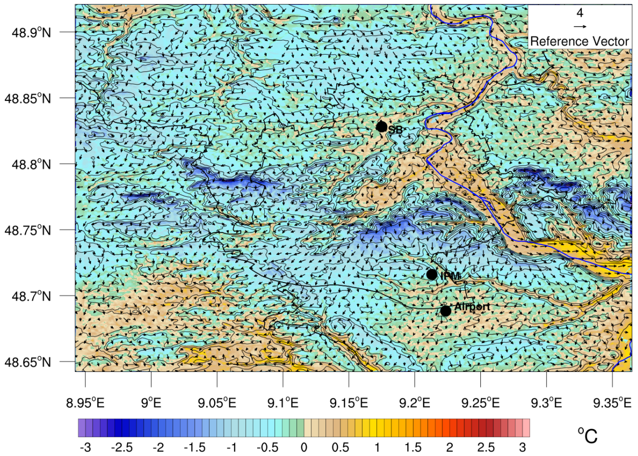

Figure 8. The 2 m temperature together with 10 m wind velocities at 12:00 UTC on 21 January 2019. The thick black line denotes the Stuttgart city limits and the thin black contour lines denote the terrain. The blue line denotes the Neckar River (river data © OpenStreetMap contributors 2020. Distributed under a Creative Commons BY-SA License).

A possible reason for the larger differences at the airport and IPM before (after) sunrise (sunset) is the observed occurrence of low stratus or fog. At the beginning of the simulation, cloud coverage was reported by 5–7 oktas (broken clouds) over Schnarrenberg and the airport at approximately 500 m a.g.l. (not shown), while after 04:00 UTC the low-level clouds started to diminish at Schnarrenberg, leading to a strong cooling until the early morning, which is seen as a temperature decrease in the observations shown in Fig. 9. The temperature drop at Schnarrenberg and IPM is also simulated but with a delay of approximately 2 h. A reason for this delayed temperature drop could be a simulated thin cloud layer around 1000 m a.g.l., which is present in the lower left and partly the lower right quadrant of the model domain. This cloud layer slowly moves in a southeasterly direction and starts to dissolve around 06:00 UTC.

During the evening transition and the following night, the low stratus develops again at the measurement sites with a ceiling of 500 m a.g.l. but is not simulated and thus contributes to a stronger cooling in the model. Another contributing factor to the delayed cloud dissipation could be the turbulence spin-up time (Kealy et al., 2019), but this is beyond the scope of this study.

Although no measurements of sensible heat and ground heat fluxes are available, diurnal cycles of the fluxes at the locations IPM, Schnarrenberg, airport, and Schlossplatz were investigated. Figure 10 shows the simulated surface sensible heat and ground heat flux at the four sites.

The sensible heat flux (Fig. 10a) shows a typical diurnal cycle with fluxes around zero before (after) sunrise (sunset). During the day, the model simulates typical wintertime sensible heat fluxes between 40 and 100 $\mathrm{W\,m^{-2}}$ (e.g., Zieliński et al., 2018), which nicely shows a dependency on the different underlying land cover types. Lower sensible heat fluxes occur over the sparsely vegetated surface at the airport as compared to the cropland station IPM, while the urban locations (Schnarrenberg and Schlossplatz) show interjacent values. As the algorithm to diagnose the 2 m temperature in Noah-MP is rather complex, no clear correlation between SH and the 2 m temperature shown in Fig. 9 can be made. The latent heat fluxes (not shown) are almost zero at Schnarrenberg and less than 10 $\mathrm{W\,m^{-2}}$ at the other two locations due to cold and dry winter conditions.

The simulated ground heat flux (Fig. 10b) shows an interesting behavior. Until sunrise, the simulated GRDFLX at the airport and IPM shows fluctuations around $-50\ \mathrm{W\,m^{-2}}$, indicating some low-level clouds in accordance with the too-high simulated 2 m temperatures shown in Fig. 9. During the further course of the day, IPM and airport show a clear diurnal cycle with maximum values between 100 and 170 $\mathrm{W\,m^{-2}}$ reflected in the highest surface temperatures during the day (not shown).

At Schnarrenberg, most of the time the ground heat flux is less than zero, indicating a cooling of the soil, while between 12:00 and 16:00 UTC small positive values are simulated. As Schnarrenberg is categorized as a low-density residential area (category 31) with an urban fraction of 0.5 and the UCM is applied here, energy is mainly stored in the urban canopy layer instead of being transferred into the soil. At Schlossplatz (high-density residential area), the ground heat flux shows a similar shape but with a larger amplitude compared to Schnarrenberg.

As this day was characterized by a shallow PBL and a temperature inversion, it is worth investigating the PBL evolution during the day. Figure 11a and b show time–height cross sections of potential temperature at IPM (top) and Schnarrenberg (bottom).

Both locations are characterized by a very stable shallow boundary layer until 09:00 UTC with a depth of less than 200 m. Between 03:00 and 09:00 UTC, the temperatures at Schnarrenberg are up to 1.5 K colder near the surface (Fig. 9), resulting in a stronger potential temperature gradient up to 400 m a.g.l. compared to the IPM location. During the day, the boundary layer height increases to 400 m a.g.l., as indicated by the constant potential temperature (e.g., Bauer et al., 2020), which is a typical value for European winter conditions (Seidel et al., 2012; Wang et al., 2020). The PBL heights are also visible by the potential temperature gradients ($\Delta\theta$) shown in Fig. 11c and d. During the morning hours, a very shallow boundary layer was simulated at Schnarrenberg (blue colors in Fig. 11c), while at IPM some fluctuations are present. During daytime, $\Delta\theta$ nicely shows the PBL height evolution up to 400 m a.g.l., while after sunset the PBL collapses to a very stable layer again (dark blue colors in Fig. 11c and d) with heights between 50–100 m a.g.l. Calculating the gradient Richardson number (*Ri*; Chan, 2008) (not shown) and assuming a threshold of 0.25 for a turbulent PBL

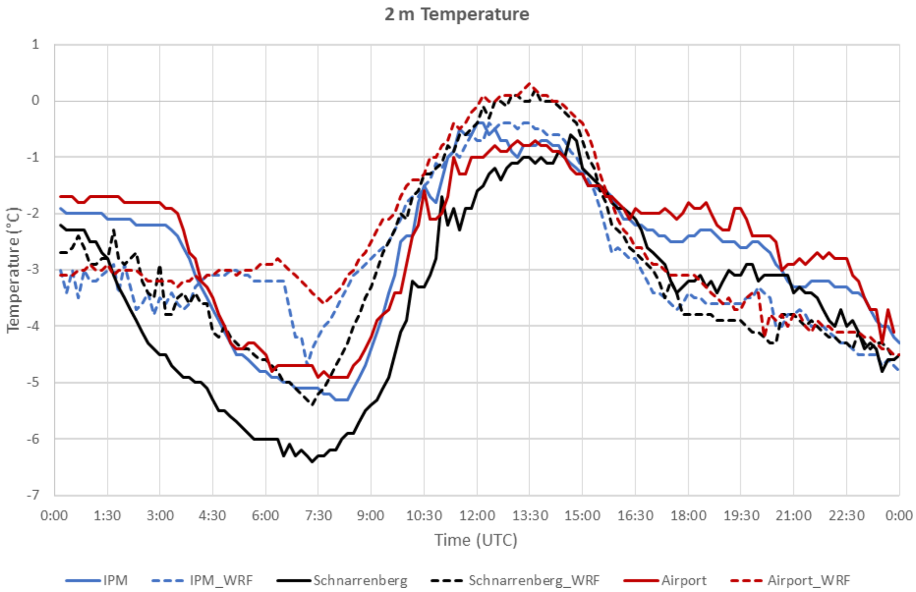

Figure 9. Diurnal cycle of 2 m temperatures for the three meteorological stations shown in Fig. 1b. Solid lines denote the observation; dashed lines denote the model simulation. The temporal resolution of the data points is 10 min.

(Seidel et al., 2012; Lee and Wekker, 2016) leads to similar results After sunset at around 15:30 UTC, the boundary layer collapses to a nighttime stable boundary layer and a temperature inversion occurs again.

4.2 Evaluation of NO_2 and PM_{10}

The most relevant air pollutants for air quality considerations in cities are NO_2 and PM_{10}. Sources for these are mainly truck supply, transit, and commuter traffic through the city as well as advection from motorways south, west, and northwest of Stuttgart.

As the incorporated emissions are from 2014 and are based on annual values, it cannot be expected that the model exactly matches the observed concentrations. For instance, the actual traffic, the sequence of traffic lights, and traffic congestions of this particular day cannot be realistically represented. In addition, all diagnosed or prognostic chemical quantities are only available on model levels. For TP applications with WRF, selecting the lowest model half level being at ~ 15 m above ground is a reasonable choice (Bauer et al., 2020).

We start with the discussion of the simulated horizontal distributions followed by vertical cross sections of NO_2 and PM_{10}.

4.2.1 Horizontal distribution

Figure 12 shows the horizontal distribution of the NO_2 concentration at the lowest model half level (~ 15 m a.g.l.) at four time steps (07:30, 12:00, 18:00, and 23:00 UTC) on 21 January 2019.

At 07:30 UTC, the morning traffic rush hour is visible in the NO_2 concentrations in Fig. 12a. High NO_2 concentrations of more than 80 $\mu g\,m^{-3}$ are simulated along the A81 motorway in the northwest of the domain, over the airport and over downtown Stuttgart. In the Neckar Valley, the concentrations exceed 120 $\mu g\,m^{-3}$. At noon (Fig. 12b), when turbulence is fully evolved (Fig. 11), the simulated NO_2 concentrations are less than 30 $\mu g\,m^{-3}$ on average apparently due to vertical mixing of NO_2 (see the next section). In the evening (Fig. 12c), the simulated NO_2 concentrations increase again, showing values of more than 100 $\mu g\,m^{-3}$ over the airport and more than 150 $\mu g\,m^{-3}$ in downtown Stuttgart and the Neckar Valley due to road and air traffic. The high morning concentrations along the northwestern motorway are not reached since the wind speed increases and the near-surface winds turn towards a westerly direction. According to the emission data set converted by the temporal factors, the evening traffic spreads over a longer time. During the night (Fig. 12d), NO_2 accumulates in the Stuttgart basin as well as the Neckar Valley due to the very low nocturnal boundary layer height of less than 200 m capped by an atmospheric inversion (Fig. 11).

Compared to the observed NO_2 concentrations (Fig. 5a), the simulated concentrations during the peak traffic times are too high at Arnulf-Klett Platz, Neckartor, and Hohenheimer Strasse. Possible reasons are that either the traffic is reduced and/or that the vehicle emission classifications have been improved since 2014. Another contributing factor could be that the vertical mixing near the surface is too weak during sunrise and sunset, while it appears slightly too strong during daytime, as indicated by the very low simulated NO_2 concentrations.

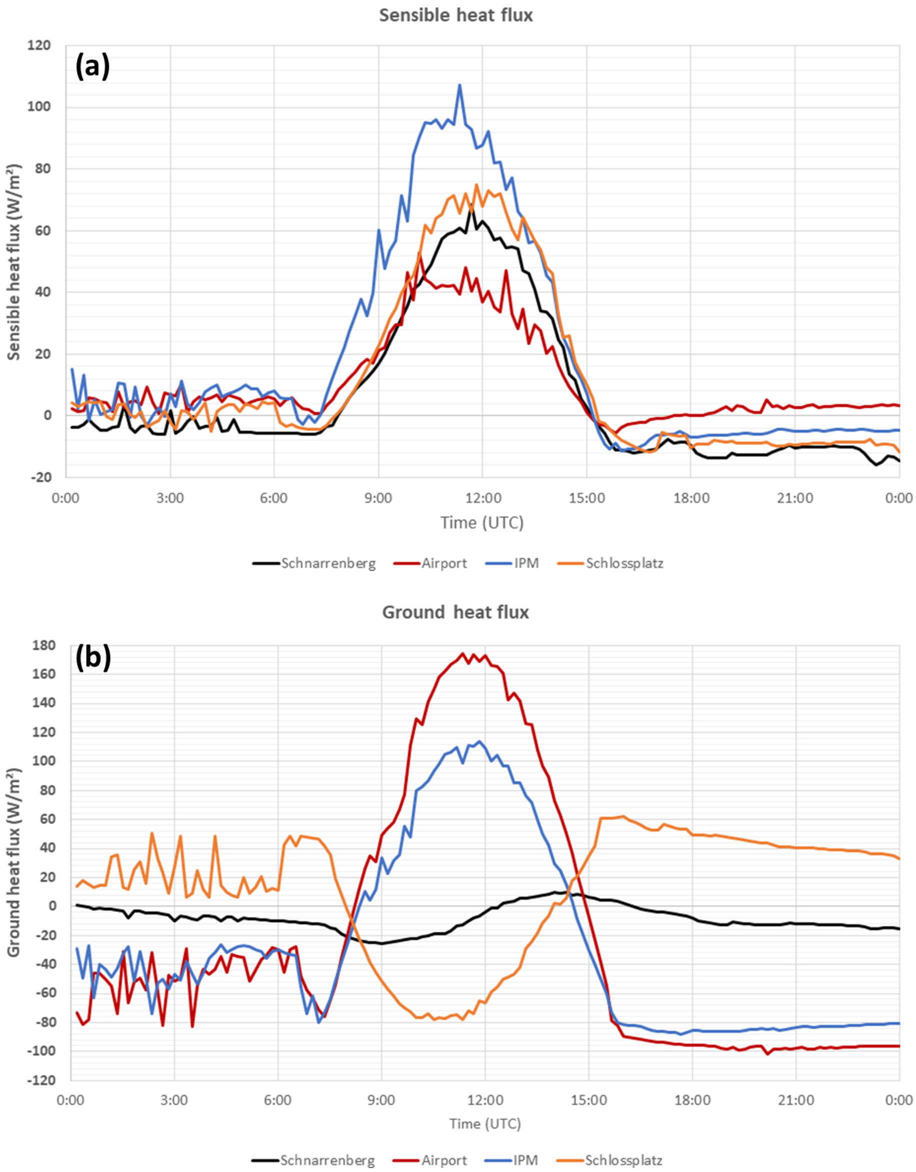

Figure 10. Diurnal cycle of simulated sensible heat flux (SH, **a**) and ground heat flux (GRDFLX, **b**) at the four stations: Schnarrenberg, Stuttgart Airport, IPM, and Schlossplatz (Fig. 1b). Positive values of GRDFLX indicate fluxes into the soil. The land cover categories are bare soil (airport), croplands (IPM), low-density residential (Schnarrenberg), and high-density residential (Schlossplatz).

Apart from NO_2, the concentration of PM_{10} is an important parameter for air quality considerations and is the decisive factor for proclaiming a "fine dust alarm" situation in Stuttgart (Stuttgart Municipality and German Meteorological Service (DWD), 2019).

Figure 13 shows the horizontal distribution of PM_{10} for the same time steps as those shown in Fig. 12.

During the morning traffic (Fig. 13a), PM_{10} accumulates in the Stuttgart basin, as this is an area with heavy traffic during the morning and an atmospheric inversion is present (Fig. 7). Interestingly, the high NO_2 concentrations along the motorway (Fig. 12a) do not lead to very high PM_{10} concentrations potentially due to chemical transitions caused by low temperatures.

During daytime, when turbulence is fully evolved, the concentration of PM_{10} decreases to less than $20\,\mu g\,m^{-3}$ due to vertical mixing and horizontal transport (see the next section). After sunset (Fig. 13c), PM_{10} starts to accumulate again in the Stuttgart basin showing concentrations between 35–$40\,\mu g\,m^{-3}$. During the night (Fig. 13d), PM_{10} accumulates over a large part of the model domain as the nocturnal boundary layer is very shallow, an inversion layer is present 200 m a.g.l., and the wind direction changes from north to west. In the configuration we use in our study, PM_{10} is a diagnostic variable, which is a sum of the $PM_{2.5}$ concen-

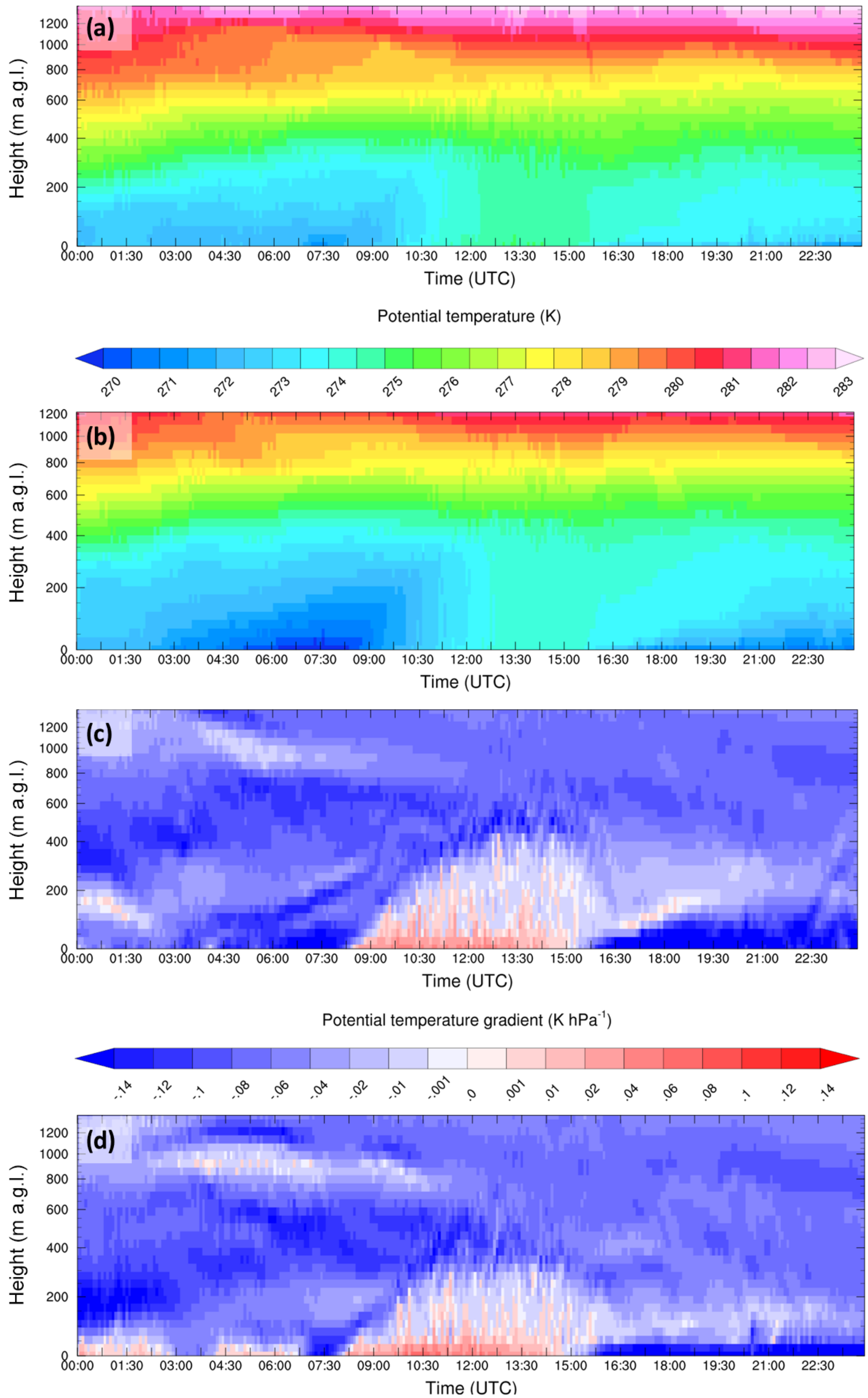

Figure 11. Time–height cross section of the simulated potential temperature at Schnarrenberg **(a)** and IPM **(b)**. Panels **(c)** and **(d)** show the potential temperature gradient at Schnarrenberg **(c)** and IPM **(d)**. The displayed altitude is above ground level.

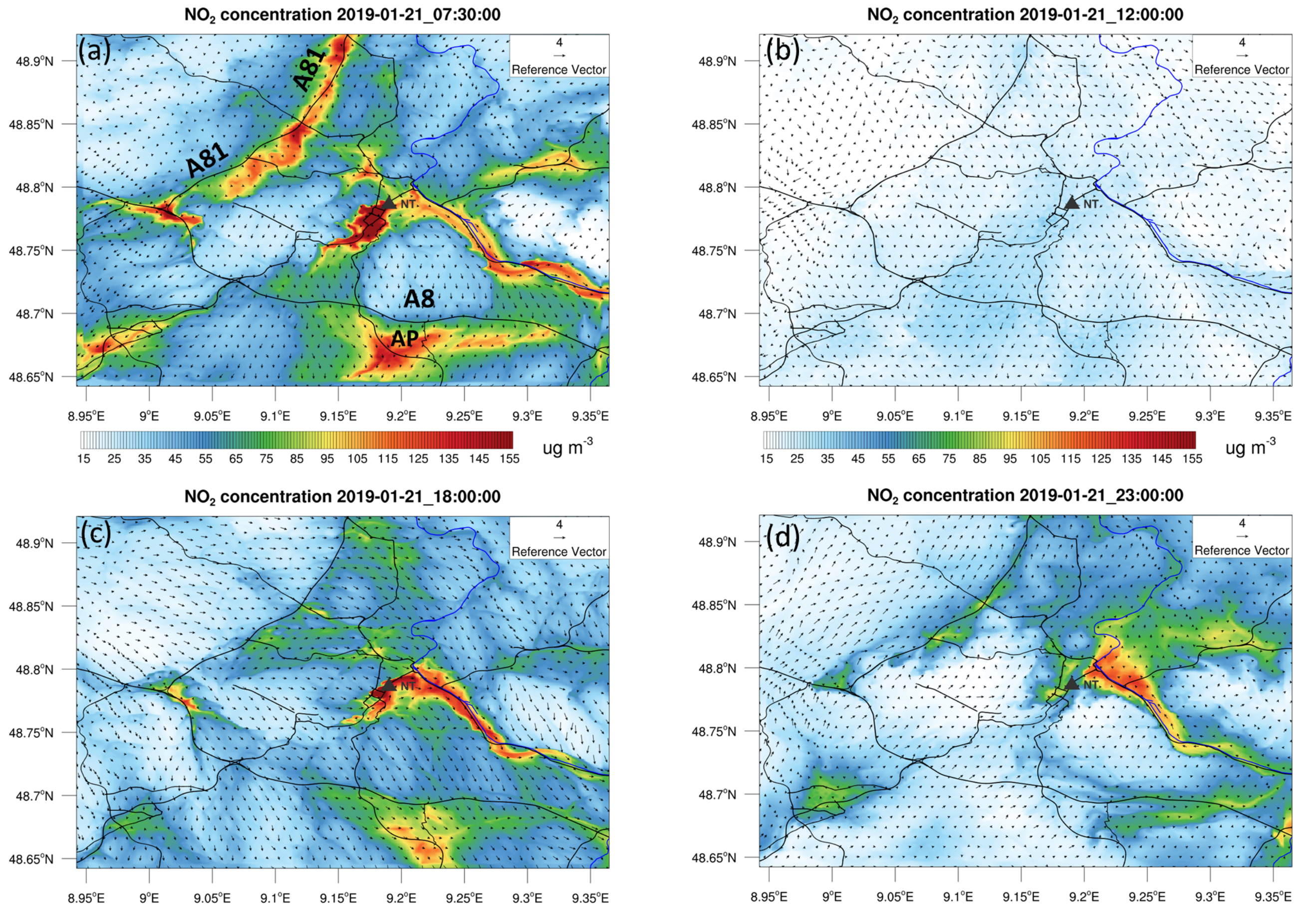

Figure 12. NO_2 concentration at the lowest model level for 07:30, 12:00, 18:00, and 23:00 UTC (**a–d**) on 21 January 2019. The black contour lines denote main roads and motorways in and around Stuttgart (map data © OpenStreetMap contributors 2020. Distributed under a Creative Commons BY-SA License). AP denotes the airport; A8 and A81 denote the main motorways around Stuttgart.

tration (which is around 26 $\mu g\,m^{-3}$ at 23:00 UTC) and the other prognostic aerosol species. As the night is very cold with temperatures far below freezing and the humidity is very high, the high concentrations could imply a very (too) strong deposition or be the result of a combination of dense evening traffic and fog formation due to weak near-surface winds.

4.2.2 Vertical distribution of NO_2 and PM_{10}

In addition to the horizontal distribution of near-surface NO_2 and PM_{10}, TP simulations with a fine vertical resolution also enable qualitative insights into the vertical distribution of pollutants. Figure 14 shows west–east cross sections at Neckartor (Fig. 1b) during the morning rush hour and at noon. Neckartor is one of the heaviest traffic locations in the Stuttgart city area.

The NO_2 concentration during the morning rush hour shows an accumulation along the motorway (red arrow in Fig. 14a) and in the region around Neckartor (white arrow in Fig. 14a), with concentrations exceeding 100 $\mu g\,m^{-3}$ as the atmospheric inversion prevents exchange with the layers above (Fig. 7). The vertical extent of concentrations higher than 30 $\mu g\,m^{-3}$ is about 200 m a.g.l. with a strong reduction above.

At noon (Fig. 14b), the simulated NO_2 concentration is much lower (less than 30 $\mu g\,m^{-3}$) as turbulence leads to a stronger mixing throughout the boundary layer up to 400 m a.g.l., which is in accordance with the simulated potential temperature time series shown in Fig. 11.

Figure 15a displays the simulated PM_{10} concentrations during the morning rush hour. Like for NO_2, higher concentrations of more than 25 $\mu g\,m^{-3}$ are simulated along the motorway and in the Stuttgart basin. During the day, PM_{10} is vertically mixed, showing a clear gradient around 800 m a.s.l. (Fig. 15b), while concentrations remain between 10–20 $\mu g\,m^{-3}$ within the boundary layer.

Apart from the west–east cross sections, it is also worthwhile to investigate the vertical temporal evolution of NO_2 and PM_{10} concentrations. Therefore, Fig. 16 shows time–height cross sections of NO_2 (top) and PM_{10} (bottom) at Neckartor.

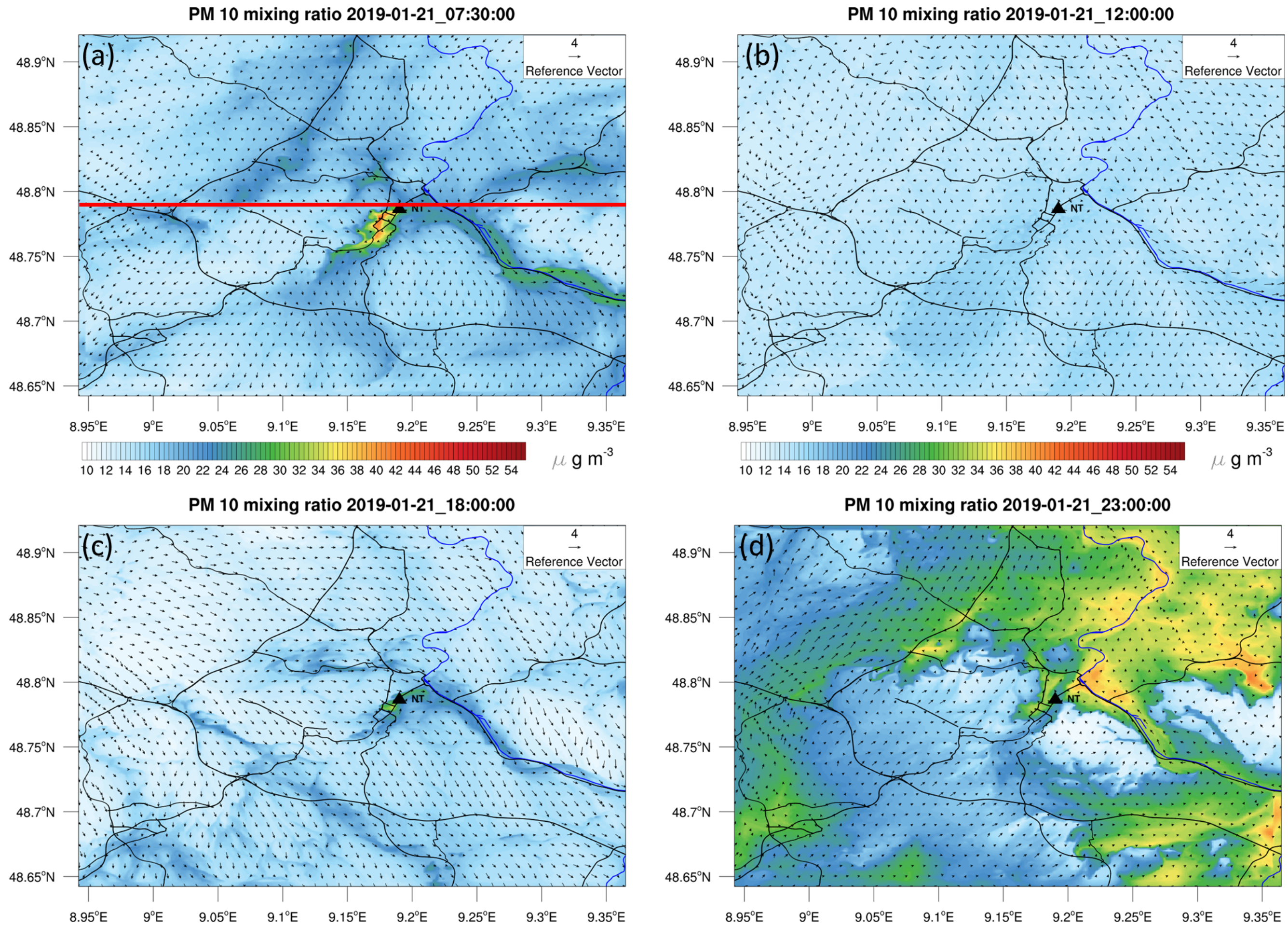

Figure 13. Same as Fig. 12 but for PM_{10} (map data © OpenStreetMap contributors 2020. Distributed under a Creative Commons BY-SA License). The red line in panel **(a)** denotes the cross section shown in Figs. 14 and 15.

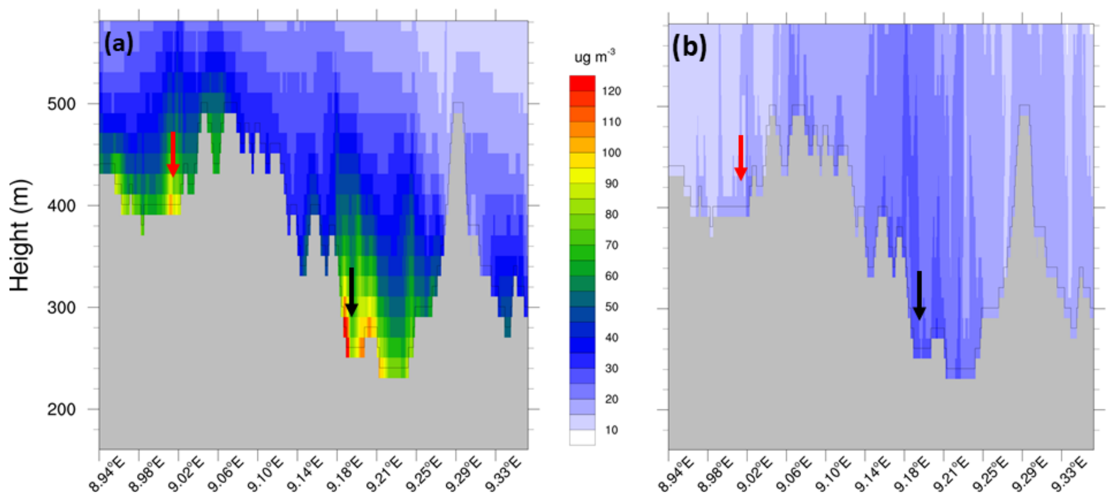

Figure 14. West–east cross section through Neckartor displaying the NO_2 concentration at 07:30 UTC **(a)** and 12:00 UTC **(b)** on 21 January 2019. The red arrow denotes the A81 motorway and the black arrow denotes the Neckartor location. The gray area shows the model terrain above mean sea level.

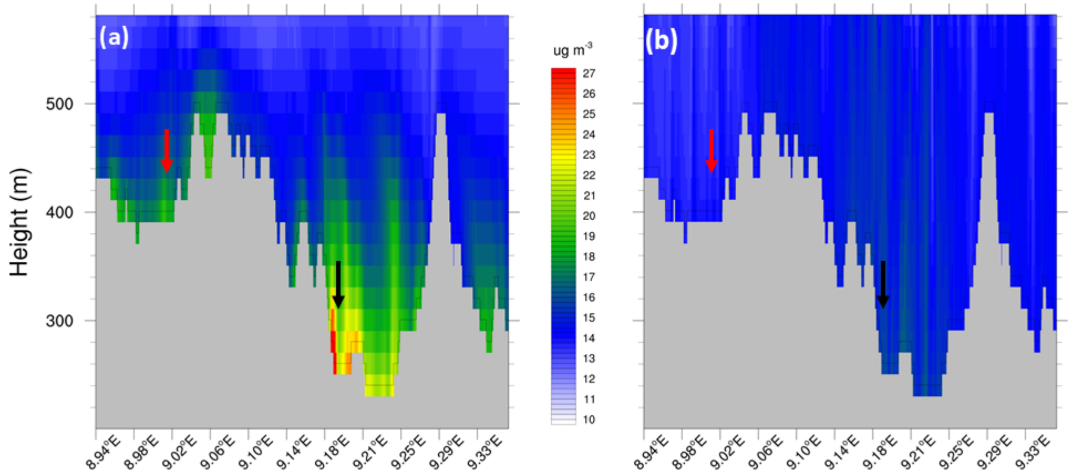

Figure 15. Same as Fig. 14 but for PM_{10}.

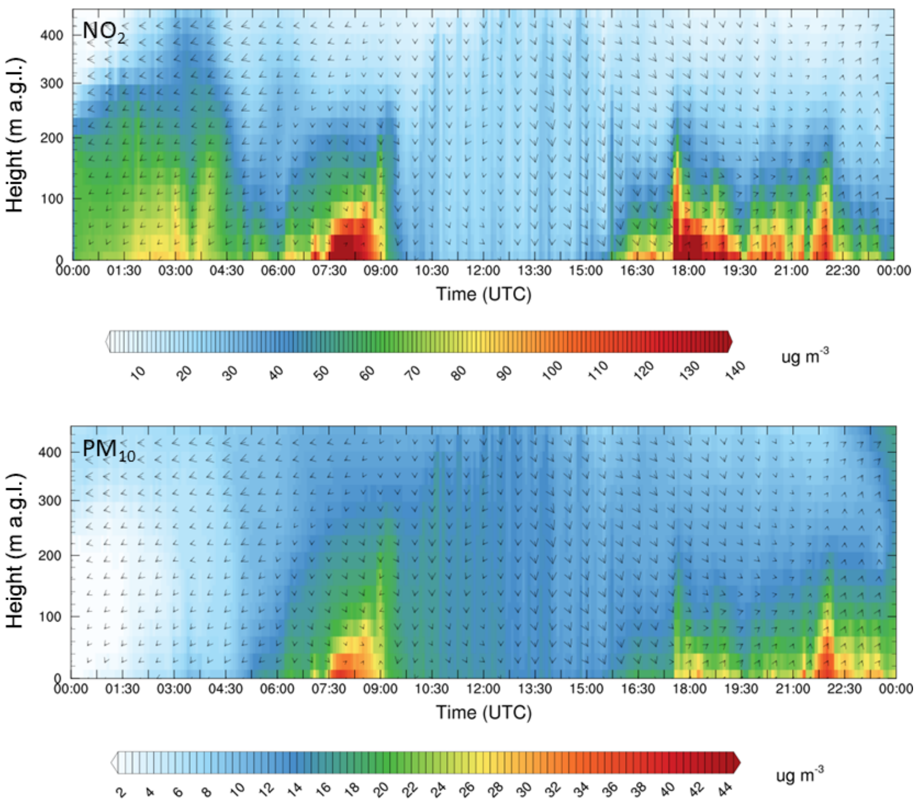

Figure 16. Time–height cross section of NO_2 (top) and PM_{10} (bottom) at Neckartor (NT) up to an altitude of 450 m a.g.l.

Well visible are the high simulated NO_2 and PM_{10} concentrations during the morning rush hour, with peak values of more than $120\,\mu g\,m^{-3}$ NO_2 and more than $40\,\mu g\,m^{-3}$ PM_{10}. The high concentrations of NO_2 and PM_{10} are present up to around 150–200 m a.g.l. During daytime, turbulence efficiently mixes the pollutants to higher altitudes, and the near-surface concentrations are quickly reduced. During the evening when the very shallow boundary layer has developed again and evening traffic commences, the particle concentrations increase, and peak values of more than $30\,\mu g\,m^{-3}$ are simulated below 100 m a.g.l.

5 Summary and conclusion

This paper describes the setup of an AQFS prototype using WRF-Chem for the Stuttgart metropolitan area. Because of the complex topography in this region, this simulation system requires a very high horizontal resolution down to the TP scale to represent all orographic and land cover features.

For the development of this prototype, 21 January 2019 served as the test case, as this was a typical winter day with an atmospheric inversion. In addition, this day was characterized as “fine dust alarm” situation, where the PM_{10} concentration at the station Neckartor in the Stuttgart basin was expected to exceed $30\,\mu g\,m^{-3}$ (http://www.stadtklima-stuttgart.de/stadtklima_filestorage/download/luft/Feinstaubwerte-2019_AN.pdf, last access: 23 March 2021). The model setup encompassed three domains down to a TP resolution of 50 m.

The initial conditions were provided by the ECMWF operational analysis, the CAMS reanalysis, and WACCM model for background chemistry. Emission data sets from CAMS-REG-AP and high-resolution data with 500 m resolution from LUBW were combined to be used in the AQFS. As current emission data sets only provide annual totals or means, a temporal decomposition following TNO was applied (Denier van der Gon et al., 2011).

For this case study, we focused on the results with respect to 2 m temperature, surface fluxes, and boundary layer evolution as well as horizontal and vertical distributions of NO_2 and PM_{10}.

Our results revealed that despite the complex topography in Stuttgart, the model is in general able to simulate a realistic diurnal cycle of 2 m temperatures, although, compared to observations, differences of up to 1 K occur. Apparently, the model has difficulties with the dissolution of low stratus clouds between 03:00 and 06:00 UTC, which was also reported in the work of Steeneveld et al. (2015), resulting in a warm 2 m temperature bias during the morning. Although no measurements are available, the surface sensible heat fluxes show a clear diurnal cycle with the magnitude clearly depending on the underlying land cover type. The low simulated ground heat flux and its fluctuations between 00:00 UTC and sunrise partially confirm the fog dissolution issue, but more test cases are needed for a more detailed investigation. Over grid cells where the single-layer UCM is active, most of the ground heat flux is stored in the canopy layer thus not transferred into the soil. The high vertical resolution of 100 levels enables a realistic representation of the nocturnal and daytime temperature inversion with an accompanying shallow boundary layer of less than 400 m during the day.

The simulation of PM_{10} shows an exceedance of the $30\,\mu g\,m^{-3}$ concentration threshold close to the Neckartor station and also fulfills the other fine dust alarm criteria shown in Sect. 3. Compared to the usually unevenly distributed air quality measurements, the AQFS allows further insights into the spatiotemporal pollutant distribution. The horizontal distributions of NO_2 and PM_{10} on this particular day clearly indicate the main polluted areas along the motorways and in the Stuttgart basin. The special orography of Stuttgart with its basin favors the accumulation of NO_2 and PM_{10} in the morning and evening, while the pollutants are well mixed to around 200–400 m a.g.l. when the boundary layer is fully evolved.

The simulation also shows that pollutants can be advected from the A81 motorway towards Stuttgart, depending on the wind situation, potentially leading to an increase of the NO_2 and partially PM_{10} concentrations in the Stuttgart basin. As can be seen from Figs. 12 and 13, the Neckar Valley can also have a large impact on the pollutant concentration in the Stuttgart basin if an atmospheric inversion together with prevailing easterly winds is present.

This is, to our knowledge, the first study of applying WRF-Chem on a TP resolution for an urban area. To derive more robust conclusions with respect to air pollution, more cases studies with different weather situations during winter and summertime are necessary. Nevertheless, our evaluation gives the following indications to further improve the quality of such simulations:

I. applying high-spatial-resolution and high-temporal-resolution gridded emission data from all pollution sources in near-real time to avoid extrapolating annual emissions to individual days (this will help to enhance the simulation of the diurnal cycles of chemical species);

II. improving the chemical background, e.g., by applying higher resolution products from the CAMS European air quality project (Marécal et al., 2015) (this will help to have a more detailed structure of the chemical constituents beneficial for subsequent downscaling simulations);

III. using a longer spin-up period and applying a larger TP model domain to further improve the spin-up of turbulence in the model;

IV. considering vertical distribution of surface emissions (e.g., Bieser et al., 2011; Guevara et al., 2021);

V. considerably increasing the number of pollutant measurements to allow more robust conclusions.

The AQFS has a great potential for urban planning applications. For example, land cover could be changed from urban low density to urban high density to investigate the impact of urban re-densification, e.g., on temperature and air quality. Although no BEP can be applied on the TP resolution with our combination of parameterizations, changes of the parameters required for the single-layer UCM offer the opportunity to perform sensitivity analysis with respect to different building heights, urban greening effects (Fallmann et al., 2016), or anthropogenic heating (Karlický et al., 2020). Recently, Lin et al. (2020) developed an interface to use output from high-resolution WRF simulations to force PALM 6.0 in an offline mode, which could be another tool in the future to study microscale structures in urban areas.

In the future, more emphasis should also be put on an improvement of the I/O (e.g., by means of quilting) and additional OpenMP capabilities in WRF-Chem. However, simulations with WRF-Chem at the TP resolution will still require around 1500–2000 compute cores for operational use due to the small numerical time step necessary.

Although air quality modeling on the TP scale is a very challenging and a computationally expensive task, we are convinced that the AQFS will have great potential to further improve process understanding and will certainly help politicians make decisions on a more scientifically valid basis.

Code and data availability. The WRF-Chem code (version 4.0.3) can be downloaded from https://github.com/wrf-model/WRF/archive/v4.0.3.tar.gz (last access: 23 March 2021) (WRF, 2021). ECMWF analysis data can be obtained from https://apps.ecmwf.int/archive-catalogue/?type=an&class=od&stream=oper&expver=1 (last access: 26 August 2020) (ECMWF, 2020). The user's affiliation needs to belong to an ECMWF member state to benefit from this data set. Due to restrictions on the input data sets for this simulation, the simulation data can only be made available upon special request from the corresponding author.

Video supplement. The video shows the simulated diurnal evolution of the NO_2 concentration (Schwitalla, 2021a) and PM_{10} concentration (Schwitalla, 2021b) over the Stuttgart metropolitan area.

Supplement. The supplement related to this article is available online at: https://doi.org/10.5194/acp-21-4575-2021-supplement.

Author contributions. TS prepared all emission data, set up the model, and performed the simulation supported by HSB. HSB reclassified the CORINE land use data set. KWS and TB conceived the idea and coordinated the project with VW. TS prepared all figures and wrote the manuscript with input from all authors. All authors equally contributed to the scientific discussion and helped to shape the research.

Competing interests. The authors declare that they have no conflict of interest.

Acknowledgements. This study has been performed within the EU-funded "Open Forecast" project (action no. 2017-DE-IA-0170). We acknowledge ECMWF for providing access to the operational IFS analysis and the CAMS reanalysis data. The Emissions of atmospheric Compounds and Compilation of Ancillary Data (ECCAD) system is acknowledged for providing the CAMS-REG-AP emission data set. We acknowledge the use of the WRF-Chem preprocessor tool MOZBC, provided by the Atmospheric Chemistry Observations and Modeling Lab (ACOM) of NCAR. The LUBW is highly acknowledged for providing high-resolution annual emission data and for the high-resolution land cover data. Joachim Ingwersen from the Department of Biogeophysics at the University of Hohenheim is acknowledged for converting the soil texture data. Joachim Fallmann from the University of Mainz is acknowledged for providing the necessary code enhancement of the dry deposition driver module to correctly couple the urban canopy model. The simulation was performed on the Cray XC40 Hazel Hen national supercomputer at the High Performance Computing Center Stuttgart (HLRS) within the WRFSCALE project. We acknowledge the editor, Ronald Cohen, and three anonymous referees for their valuable comments that helped to improve the quality of the paper.

Financial support. This research has been supported by the Connecting Europe Facility initiative of the European Union (action no. 2017-DE-IA-0170).

Review statement. This paper was edited by Ronald Cohen and reviewed by three anonymous referees.

References

Ackermann, I. J., Hass, H., Memmesheimer, M., Ebel, A., Binkowski, F. S., and Shankar, U.: Modal aerosol dynamics model for Europe, Atmos. Environ., 32, 2981–2999, https://doi.org/10.1016/S1352-2310(98)00006-5, 1998.

Baldauf, M., Seifert, A., Förstner, J., Majewski, D., Raschendorfer, M., and Reinhardt, T.: Operational Convective-Scale Numerical Weather Prediction with the COSMO Model: Description and Sensitivities, Mon. Weather Rev., 139, 3887–3905, https://doi.org/10.1175/MWR-D-10-05013.1, 2011.

Barker, D., Huang, X.-Y., Liu, Z., Auligné, T., Zhang, X., Rugg, S., Ajjaji, R., Bourgeois, A., Bray, J., Chen, Y., Demirtas, M., Guo, Y.-R., Henderson, T., Huang, W., Lin, H.-C., Michalakes, J., Rizvi, S., and Zhang, X.: The Weather Research and Forecasting Model's Community Variational/Ensemble Data Assimilation System: WRFDA, B. Am. Meteorol. Soc., 93, 831–843, https://doi.org/10.1175/BAMS-D-11-00167.1, 2012.

Bauer, H.-S., Muppa, S. K., Wulfmeyer, V., Behrendt, A., Warrach-Sagi, K., and Späth, F.: Multi-nested WRF simulations for studying planetary boundary layer processes on the turbulence-permitting scale in a realistic mesoscale environment, Tellus A, 72, 1–28, https://doi.org/10.1080/16000870.2020.1761740, 2020.

Bieser, J., Aulinger, A., Matthias, V., Quante, M., and van der Denier Gon, H. A. C.: Vertical emission profiles for Europe based on plume rise calculations, Environ. Pollut. (Barking, Essex 1987), 159, 2935–2946, https://doi.org/10.1016/j.envpol.2011.04.030, 2011.

Bonavita, M., Hólm, E., Isaksen, L., and Fisher, M.: The evolution of the ECMWF hybrid data assimilation system, Q. J. Roy. Meteor. Soc., 142, 287–303, https://doi.org/10.1002/qj.2652, 2016.

Brasseur, G. P., Hauglustaine, D. A., Walters, S., Rasch, P. J., Müller, J.-F., Granier, C., and Tie, X. X.: MOZART, a global chemical transport model for ozone and related chemical tracers: 1. Model description, J. Geophys. Res., 103, 28265–28289, https://doi.org/10.1029/98JD02397, 1998.

Butcher, G., Barnes, C., and Owen, L.: Landsat: The cornerstone of global land imaging, GIM International, January/February, 31–35, available at: http://pubs.er.usgs.gov/publication/70202363 (last access: 23 March 2021), 2019.

Chan, P. W.: Determination of Richardson number profile from remote sensing data and its aviation application, IOP Conf. Ser.: Earth Environ. Sci., 1, 12043, https://doi.org/10.1088/1755-1315/1/1/012043, 2008.

Chen, D., Liu, Z., Ban, J., Zhao, P., and Chen, M.: Retrospective analysis of 2015–2017 wintertime $PM_{2.5}$ in China: response to emission regulations and the role of meteorology, Atmos. Chem. Phys., 19, 7409–7427, https://doi.org/10.5194/acp-19-7409-2019, 2019.

Copernicus: Copernicus official website, available at: https://atmosphere.copernicus.eu/ (last access: 21 July 2020), 2020.

Coppola, E., Sobolowski, S., Pichelli, E., Raffaele, F., Ahrens, B., Anders, I., Ban, N., Bastin, S., Belda, M., Belusic, D., Caldas-Alvarez, A., Cardoso, R. M., Davolio, S., Dobler, A., Fernandez, J., Fita, L., Fumiere, Q., Giorgi, F., Goergen, K., Güttler, I., Halenka, T., Heinzeller, D., Hodnebrog, Ø., Jacob, D., Kartsios, S., Katragkou, E., Kendon, E., Khodayar, S., Kunstmann, H., Knist, S., Lavín-Gullón, A., Lind, P., Lorenz, T., Maraun, D., Marelle, L., van Meijgaard, E., Milovac, J., Myhre, G., Panitz, H.-J., Piazza, M., Raffa, M., Raub, T., Rockel, B., Schär, C., Sieck, K., Soares, P. M. M., Somot, S., Srnec, L., Stocchi, P., Tölle, M. H., Truhetz, H., Vautard, R., Vries, H. de, and Warrach-Sagi, K.: A first-of-its-kind multi-model convection permitting ensemble for investigating convective phenomena over Europe and the Mediterranean, Clim. Dynam., 55, 3–34, https://doi.org/10.1007/s00382-018-4521-8, 2020.

Corsmeier, U., Kalthoff, N., Barthlott, C., Aoshima, F., Behrendt, A., Di Girolamo, P., Dorninger, M., Handwerker, J., Kottmeier, C., Mahlke, H., Mobbs, S. D., Norton, E. G., Wickert, J., and Wulfmeyer, V.: Processes driving deep convection over complex terrain: a multi-scale analysis of observations from COPS IOP 9c, Q. J. Roy. Meteor. Soc., 137, 137–155, https://doi.org/10.1002/qj.754, 2011.

Danielson, J. J. and Gesch, D. B.: Global multi-resolution terrain elevation data 2010 (GMTED2010), Open-File report, avasilable at: https://pubs.er.usgs.gov/publication/ofr20111073 (last access: 23 March 2021), 2011.

Denier van der Gon, H., Hendriks, C., Kuenen, J., Segers, A., and Visschedijk, A.: Description of current temporal emission patterns and sensitivity of predicted AQ for temporal emission patterns: EU FP7 MACC deliverable report D_D-EMIS_1.3, TNO report, available at: https://atmosphere.copernicus.eu/sites/default/files/2019-07/MACC_TNO_del_1_3_v2.pdf (last access: 23 March 2021), 2011.

ECMWF: Archive Catalogue, available at: https://apps.ecmwf.int/archive-catalogue/?type=an&class=od&stream=oper&expver=1, last access: 26 August 2020.

European Union: Copernicus Land Monitoring Service 2012, European Environment Agency, Copenhagen, Denmark, 2012.

European Union: Copernicus Land Monitoring Service 2017, European Environment Agency, Copenhagen, Denmark, 2017.

Fallmann, J.: Numerical simulations to assess the effect of urban heat island mitigation strategies on regional air quality, PhD Thesis, Universität zu Köln, Cologne, 2014.

Fallmann, J., Emeis, S., and Suppan, P.: Mitigation of urban heat stress – a modelling case study for the area of Stuttgart, DIE ERDE – Journal of the Geographical Society of Berlin, 144, 202–216, https://doi.org/10.12854/erde-144-15, 2014.

Fallmann, J., Forkel, R., and Emeis, S.: Secondary effects of urban heat island mitigation measures on air quality, Atmos. Environ., 125, 199–211, https://doi.org/10.1016/j.atmosenv.2015.10.094, 2016.

Farr, T. G., Rosen, P. A., Caro, E., Crippen, R., Duren, R., Hensley, S., Kobrick, M., Paller, M., Rodriguez, E., Roth, L., Seal, D., Shaffer, S., Shimada, J., Umland, J., Werner, M., Oskin, M., Burbank, D., and Alsdorf, D.: The Shuttle Radar Topography Mission, Rev. Geophys., 45, RG2004, https://doi.org/10.1029/2005RG000183, 2007.

Flemming, J., Huijnen, V., Arteta, J., Bechtold, P., Beljaars, A., Blechschmidt, A.-M., Diamantakis, M., Engelen, R. J., Gaudel, A., Inness, A., Jones, L., Josse, B., Katragkou, E., Marecal, V., Peuch, V.-H., Richter, A., Schultz, M. G., Stein, O., and Tsikerdekis, A.: Tropospheric chemistry in the Integrated Forecasting System of ECMWF, Geosci. Model Dev., 8, 975–1003, https://doi.org/10.5194/gmd-8-975-2015, 2015.

Forkel, R., Balzarini, A., Baró, R., Bianconi, R., Curci, G., Jiménez-Guerrero, P., Hirtl, M., Honzak, L., Lorenz, C., Im, U., Pérez, J. L., Pirovano, G., San José, R., Tuccella, P., Werhahn, J., and Žabkar, R.: Analysis of the WRF-Chem contributions to AQMEII phase2 with respect to aerosol radiative feedbacks on meteorology and pollutant distributions, Atmos. Environ., 115, 630–645, https://doi.org/10.1016/j.atmosenv.2014.10.056, 2015.

Freitas, S. R., Longo, K. M., Alonso, M. F., Pirre, M., Marecal, V., Grell, G., Stockler, R., Mello, R. F., and Sánchez Gácita, M.: PREP-CHEM-SRC – 1.0: a preprocessor of trace gas and aerosol emission fields for regional and global atmospheric chemistry models, Geosci. Model Dev., 4, 419–433, https://doi.org/10.5194/gmd-4-419-2011, 2011.

Freitas, S. R., Panetta, J., Longo, K. M., Rodrigues, L. F., Moreira, D. S., Rosário, N. E., Silva Dias, P. L., Silva Dias, M. A. F., Souza, E. P., Freitas, E. D., Longo, M., Frassoni, A., Fazenda, A. L., Santos e Silva, C. M., Pavani, C. A. B., Eiras, D., França, D. A., Massaru, D., Silva, F. B., Santos, F. C., Pereira, G., Camponogara, G., Ferrada, G. A., Campos Velho, H. F., Menezes, I., Freire, J. L., Alonso, M. F., Gácita, M. S., Zarzur, M., Fonseca, R. M., Lima, R. S., Siqueira, R. A., Braz, R., Tomita, S., Oliveira, V., and Martins, L. D.: The Brazilian developments on the Regional Atmospheric Modeling System (BRAMS 5.2): an integrated environmental model tuned for tropical areas, Geosci. Model Dev., 10, 189–222, https://doi.org/10.5194/gmd-10-189-2017, 2017.

García-Díez, M., Lauwaet, D., Hooyberghs, H., Ballester, J., De Ridder, K., and Rodó, X.: Advantages of using a fast urban boundary layer model as compared to a full mesoscale model to simulate the urban heat island of Barcelona, Geosci. Model Dev., 9, 4439–4450, https://doi.org/10.5194/gmd-9-4439-2016, 2016.

Giorgi, F., Coppola, E., Solmon, F., Mariotti, L., Sylla, M. B., Bi, X., Elguindi, N., Diro, G. T., Nair, V., Giuliani, G., Turuncoglu, U. U., Cozzini, S., Güttler, I., O'Brien, T. A., Tawfik, A. B., Shalaby, A., Zakey, A. S., Steiner, A. L., Stordal, F., Sloan, L. C., and Brankovic, C.: RegCM4: model description and preliminary tests over multiple CORDEX domains, Clim. Res., 52, 7–29, https://doi.org/10.3354/cr01018, 2012.

Granier, C., Darras, S., Denier van der Gon, H., Doubalova, J., Elguindi, N., Galle, B., Gauss, M., Guevara, M., Jalkanen, J.-P., Kuenen, J., Liousse, C., Quack, B., Simpson, D., and Sindelarova, K.: The Copernicus Atmosphere Monitoring Service global and regional emissions (April 2019 version), https://doi.org/10.24380/d0bn-kx16, 2019.

Grell, G. A., Peckham, S. E., Schmitz, R., McKeen, S. A., Frost, G., Skamarock, W. C., and Eder, B.: Fully coupled "online" chemistry within the WRF model, Atmos. Environ., 39, 6957–6975, https://doi.org/10.1016/j.atmosenv.2005.04.027, 2005.

Guevara, M., Jorba, O., Tena, C., Denier van der Gon, H., Kuenen, J., Elguindi, N., Darras, S., Granier, C., and Pérez García-Pando, C.: Copernicus Atmosphere Monitoring Service TEMPOral profiles (CAMS-TEMPO): global and European emission temporal profile maps for atmospheric chemistry modelling, Earth Syst. Sci. Data, 13, 367–404, https://doi.org/10.5194/essd-13-367-2021, 2021.

Heinze, R., Moseley, C., Böske, L. N., Muppa, S. K., Maurer, V., Raasch, S., and Stevens, B.: Evaluation of large-eddy simulations forced with mesoscale model output for a multi-week period during a measurement campaign, Atmos. Chem. Phys., 17, 7083–7109, https://doi.org/10.5194/acp-17-7083-2017, 2017a.

Heinze, R., Dipankar, A., Henken, C. C., Moseley, C., Sourdeval, O., Trömel, S., Xie, X., Adamidis, P., Ament, F., Baars, H., Barthlott, C., Behrendt, A., Blahak, U., Bley, S., Brdar, S., Brueck, M., Crewell, S., Deneke, H., Di Girolamo, P., Evaristo, R., Fischer, J., Frank, C., Friederichs, P., Göcke, T., Gorges, K., Hande, L., Hanke, M., Hansen, A., Hege, H.-C., Hoose, C., Jahns, T., Kalthoff, N., Klocke, D., Kneifel, S., Knippertz, P., Kuhn, A., van Laar, T., Macke, A., Maurer, V., Mayer, B., Meyer, C. I., Muppa, S. K., Neggers, R. A. J., Orlandi, E., Pantillon, F., Pospichal, B., Röber, N., Scheck, L., Seifert, A., Seifert, P., Senf, F., Siligam, P., Simmer, C., Steinke, S., Stevens, B., Wapler, K., Weniger, M., Wulfmeyer, V., Zängl, G., Zhang, D., and Quaas, J.: Large-eddy simulations over Germany using ICON: a comprehensive evaluation, Q. J. Roy. Meteor. Soc., 143, 69–100, https://doi.org/10.1002/qj.2947, 2017b.

Hengl, T., Jesus, J. M. de, MacMillan, R. A., Batjes, N. H., Heuvelink, G. B. M., Ribeiro, E., Samuel-Rosa, A., Kempen, B., Leenaars, J. G. B., Walsh, M. G., and Gonzalez, M. R.: SoilGrids1km–global soil information based on automated mapping, PloS one, 9, e105992, https://doi.org/10.1371/journal.pone.0105992, 2014.

Hengl, T., Heuvelink, G. B. M., Kempen, B., Leenaars, J. G. B., Walsh, M. G., Shepherd, K. D., Sila, A., MacMillan, R. A., Mendes de Jesus, J., Tamene, L., and Tondoh, J. E.: Mapping Soil Properties of Africa at 250 m Resolution: Random Forests Significantly Improve Current Predictions, PloS one, 10, e0125814, https://doi.org/10.1371/journal.pone.0125814, 2015.

Hong, S.-Y., Noh, Y., and Dudhia, J.: A New Vertical Diffusion Package with an Explicit Treatment of Entrainment Processes, Mon. Weather Rev., 134, 2318–2341, https://doi.org/10.1175/MWR3199.1, 2006.

Honnert, R. and Masson, V.: What is the smallest physically acceptable scale for 1D turbulence schemes?, Front. Earth Sci., 2, 27, https://doi.org/10.3389/feart.2014.00027, 2014.

Honnert, R., Efstathiou, G. A., Beare, R. J., Ito, J., Lock, A., Neggers, R., Plant, R. S., Shin, H. H., Tomassini, L., and Zhou, B.: The Atmospheric Boundary Layer and the "Gray Zone" of Turbulence: A Critical Review, J. Geophys. Res.-Atmos., 125, e2019JD030317, https://doi.org/10.1029/2019JD030317, 2020.

Horowitz, L. W., Walters, S., Mauzerall, D. L., Emmons, L. K., Rasch, P. J., Granier, C., Tie, X., Lamarque, J.-F., Schultz, M. G., Tyndall, G. S., Orlando, J. J., and Brasseur, G. P.: A global simulation of tropospheric ozone and related tracers: Description and evaluation of MOZART, version 2, J. Geophys. Res., 108, 4784, https://doi.org/10.1029/2002JD002853, 2003.

Huszar, P., Karlický, J., Ďoubalová, J., Šindelářová, K., Nováková, T., Belda, M., Halenka, T., Žák, M., and Pišoft, P.: Urban canopy meteorological forcing and its impact on ozone and $PM_{2.5}$: role of vertical turbulent transport, Atmos. Chem. Phys., 20, 1977–2016, https://doi.org/10.5194/acp-20-1977-2020, 2020.

Iacono, M. J., Delamere, J. S., Mlawer, E. J., Shephard, M. W., Clough, S. A., and Collins, W. D.: Radiative forcing by long-lived greenhouse gases: Calculations with the AER radiative transfer models, J. Geophys. Res., 113, D13103, https://doi.org/10.1029/2008JD009944, 2008.

Inness, A., Ades, M., Agustí-Panareda, A., Barré, J., Benedictow, A., Blechschmidt, A.-M., Dominguez, J. J., Engelen, R., Eskes, H., Flemming, J., Huijnen, V., Jones, L., Kipling, Z., Massart, S., Parrington, M., Peuch, V.-H., Razinger, M., Remy, S., Schulz, M., and Suttie, M.: The CAMS reanalysis of atmospheric composition, Atmos. Chem. Phys., 19, 3515–3556, https://doi.org/10.5194/acp-19-3515-2019, 2019.

Jiménez, P. A., Dudhia, J., González-Rouco, J. F., Navarro, J., Montávez, J. P., and García-Bustamante, E.: A Revised Scheme for the WRF Surface Layer Formulation, Mon. Weather Rev., 140, 898–918, https://doi.org/10.1175/MWR-D-11-00056.1, 2012.

Jin, L., Li, Z., He, Q., Miao, Q., Zhang, H., and Yang, X.: Observation and simulation of near-surface wind and its variation with topography in Urumqi, West China, J. Meteorol. Res.-PRC, 30, 961–982, https://doi.org/10.1007/s13351-016-6012-3, 2016.

Karlický, J., Huszár, P., Nováková, T., Belda, M., Švábik, F., Ďoubalová, J., and Halenka, T.: The "urban meteorology island": a multi-model ensemble analysis, Atmos. Chem. Phys., 20, 15061–15077, https://doi.org/10.5194/acp-20-15061-2020, 2020.

Kawabata, T., Schwitalla, T., Adachi, A., Bauer, H.-S., Wulfmeyer, V., Nagumo, N., and Yamauchi, H.: Observational operators for dual polarimetric radars in variational data assimilation systems (PolRad VAR v1.0), Geosci. Model Dev., 11, 2493–2501, https://doi.org/10.5194/gmd-11-2493-2018, 2018.

Kealy, J. C., Efstathiou, G. A., and Beare, R. J.: The Onset of Resolved Boundary-Layer Turbulence at Grey-Zone Resolutions, Bound.-Lay. Meteorol., 171, 31–52, https://doi.org/10.1007/s10546-018-0420-0, 2019.

Khan, B., Banzhaf, S., Chan, E. C., Forkel, R., Kanani-Sühring, F., Ketelsen, K., Kurppa, M., Maronga, B., Mauder, M., Raasch, S., Russo, E., Schaap, M., and Sühring, M.: Development of an atmospheric chemistry model coupled to the PALM model system 6.0: implementation and first applications, Geosci.

Model Dev., 14, 1171–1193, https://doi.org/10.5194/gmd-14-1171-2021, 2021.

Kosovic, B.: Subgrid-scale modelling for the large-eddy simulation of high-Reynolds-number boundary layers, J. Fluid Mech., 336, 151–182, https://doi.org/10.1017/S0022112096004697, 1997.

Kuenen, J. J. P., Visschedijk, A. J. H., Jozwicka, M., and Denier van der Gon, H. A. C.: TNO-MACC_II emission inventory; a multi-year (2003–2009) consistent high-resolution European emission inventory for air quality modelling, Atmos. Chem. Phys., 14, 10963–10976, https://doi.org/10.5194/acp-14-10963-2014, 2014.

Kuik, F., Lauer, A., Churkina, G., Denier van der Gon, H. A. C., Fenner, D., Mar, K. A., and Butler, T. M.: Air quality modelling in the Berlin–Brandenburg region using WRF-Chem v3.7.1: sensitivity to resolution of model grid and input data, Geosci. Model Dev., 9, 4339–4363, https://doi.org/10.5194/gmd-9-4339-2016, 2016.

Kuik, F., Kerschbaumer, A., Lauer, A., Lupascu, A., von Schneidemesser, E., and Butler, T. M.: Top–down quantification of NO_x emissions from traffic in an urban area using a high-resolution regional atmospheric chemistry model, Atmos. Chem. Phys., 18, 8203–8225, https://doi.org/10.5194/acp-18-8203-2018, 2018.

Kusaka, H. and Kimura, F.: Coupling a Single-Layer Urban Canopy Model with a Simple Atmospheric Model: Impact on Urban Heat Island Simulation for an Idealized Case, J. Meteorol. Soc. Jpn., 82, 67–80, https://doi.org/10.2151/jmsj.82.67, 2004.

Lee, T. R. and de Wekker, S. F. J.: Estimating Daytime Planetary Boundary Layer Heights over a Valley from Rawinsonde Observations at a Nearby Airport: An Application to the Page Valley in Virginia, United States, J. Appl. Meteorol. Clim., 55, 791–809, https://doi.org/10.1175/JAMC-D-15-0300.1, 2016.

Li, Z., Zhou, Y., Wan, B., Chung, H., Huang, B., and Liu, B.: Model evaluation of high-resolution urban climate simulations: using the WRF/Noah LSM/SLUCM model (Version 3.7.1) as a case study, Geosci. Model Dev., 12, 4571–4584, https://doi.org/10.5194/gmd-12-4571-2019, 2019.

Lian, J., Wu, L., Bréon, F.-M., Broquet, G., Vautard, R., Zaccheo, T. S., Dobler, J., and Ciais, P.: Evaluation of the WRF-UCM mesoscale model and ECMWF global operational forecasts over the Paris region in the prospect of tracer atmospheric transport modeling, Elem. Sci. Anth., 6, 64, https://doi.org/10.1525/elementa.319, 2018.

Lin, D., Khan, B., Katurji, M., Bird, L., Faria, R., and Revell, L. E.: WRF4PALM v1.0: A Mesoscale Dynamical Driver for the Microscale PALM Model System 6.0, Geosci. Model Dev. Discuss. [preprint], https://doi.org/10.5194/gmd-2020-306, in review, 2020.

Mailler, S., Menut, L., Khvorostyanov, D., Valari, M., Couvidat, F., Siour, G., Turquety, S., Briant, R., Tuccella, P., Bessagnet, B., Colette, A., Létinois, L., Markakis, K., and Meleux, F.: CHIMERE-2017: from urban to hemispheric chemistry-transport modeling, Geosci. Model Dev., 10, 2397–2423, https://doi.org/10.5194/gmd-10-2397-2017, 2017.

Manders, A. M. M., Builtjes, P. J. H., Curier, L., Denier van der Gon, H. A. C., Hendriks, C., Jonkers, S., Kranenburg, R., Kuenen, J. J. P., Segers, A. J., Timmermans, R. M. A., Visschedijk, A. J. H., Wichink Kruit, R. J., van Pul, W. A. J., Sauter, F. J., van der Swaluw, E., Swart, D. P. J., Douros, J., Eskes, H., van Meijgaard, E., van Ulft, B., van Velthoven, P., Banzhaf, S., Mues, A. C., Stern, R., Fu, G., Lu, S., Heemink, A., van Velzen, N., and Schaap, M.: Curriculum vitae of the LOTOS–EUROS (v2.0) chemistry transport model, Geosci. Model Dev., 10, 4145–4173, https://doi.org/10.5194/gmd-10-4145-2017, 2017.

Mar, K. A., Ojha, N., Pozzer, A., and Butler, T. M.: Ozone air quality simulations with WRF-Chem (v3.5.1) over Europe: model evaluation and chemical mechanism comparison, Geosci. Model Dev., 9, 3699–3728, https://doi.org/10.5194/gmd-9-3699-2016, 2016.

Marécal, V., Peuch, V.-H., Andersson, C., Andersson, S., Arteta, J., Beekmann, M., Benedictow, A., Bergström, R., Bessagnet, B., Cansado, A., Chéroux, F., Colette, A., Coman, A., Curier, R. L., Denier van der Gon, H. A. C., Drouin, A., Elbern, H., Emili, E., Engelen, R. J., Eskes, H. J., Foret, G., Friese, E., Gauss, M., Giannaros, C., Guth, J., Joly, M., Jaumouillé, E., Josse, B., Kadygrov, N., Kaiser, J. W., Krajsek, K., Kuenen, J., Kumar, U., Liora, N., Lopez, E., Malherbe, L., Martinez, I., Melas, D., Meleux, F., Menut, L., Moinat, P., Morales, T., Parmentier, J., Piacentini, A., Plu, M., Poupkou, A., Queguiner, S., Robertson, L., Rouïl, L., Schaap, M., Segers, A., Sofiev, M., Tarasson, L., Thomas, M., Timmermans, R., Valdebenito, Á., van Velthoven, P., van Versendaal, R., Vira, J., and Ung, A.: A regional air quality forecasting system over Europe: the MACC-II daily ensemble production, Geosci. Model Dev., 8, 2777–2813, https://doi.org/10.5194/gmd-8-2777-2015, 2015.

Maronga, B., Gryschka, M., Heinze, R., Hoffmann, F., Kanani-Sühring, F., Keck, M., Ketelsen, K., Letzel, M. O., Sühring, M., and Raasch, S.: The Parallelized Large-Eddy Simulation Model (PALM) version 4.0 for atmospheric and oceanic flows: model formulation, recent developments, and future perspectives, Geosci. Model Dev., 8, 2515–2551, https://doi.org/10.5194/gmd-8-2515-2015, 2015.

Maronga, B., Gross, G., Raasch, S., Banzhaf, S., Forkel, R., Heldens, W., Kanani-Sühring, F., Matzarakis, A., Mauder, M., Pavlik, D., Pfafferott, J., Schubert, S., Seckmeyer, G., Sieker, H., and Winderlich, K.: Development of a new urban climate model based on the model PALM – Project overview, planned work, and first achievements, Meteorol. Z., 28, 105–119, https://doi.org/10.1127/metz/2019/0909, 2019.

Maronga, B., Banzhaf, S., Burmeister, C., Esch, T., Forkel, R., Fröhlich, D., Fuka, V., Gehrke, K. F., Geletič, J., Giersch, S., Gronemeier, T., Groß, G., Heldens, W., Hellsten, A., Hoffmann, F., Inagaki, A., Kadasch, E., Kanani-Sühring, F., Ketelsen, K., Khan, B. A., Knigge, C., Knoop, H., Krč, P., Kurppa, M., Maamari, H., Matzarakis, A., Mauder, M., Pallasch, M., Pavlik, D., Pfafferott, J., Resler, J., Rissmann, S., Russo, E., Salim, M., Schrempf, M., Schwenkel, J., Seckmeyer, G., Schubert, S., Sühring, M., von Tils, R., Vollmer, L., Ward, S., Witha, B., Wurps, H., Zeidler, J., and Raasch, S.: Overview of the PALM model system 6.0, Geosci. Model Dev., 13, 1335–1372, https://doi.org/10.5194/gmd-13-1335-2020, 2020.

Marsh, D. R., Mills, M. J., Kinnison, D. E., Lamarque, J.-F., Calvo, N., and Polvani, L. M.: Climate Change from 1850 to 2005 Simulated in CESM1(WACCM), J. Climate, 26, 7372–7391, https://doi.org/10.1175/JCLI-D-12-00558.1, 2013.

Martilli, A., Clappier, A., and Rotach, M. W.: An Urban Surface Exchange Parameterisation for Mesoscale Models, Bound.-Lay. Meteorol., 104, 261–304, https://doi.org/10.1023/A:1016099921195, 2002.

Memmesheimer, M., Friese, E., Ebel, A., Jakobs, H. J., Feldmann, H., Kessler, C., and Piekorz, G.: Long-term simulations of particulate matter in Europe on different scales using sequential nesting of a regional model, Int. J. Environ. Pollut., 22, 108, https://doi.org/10.1504/IJEP.2004.005530, 2004.

Milovac, J., Warrach-Sagi, K., Behrendt, A., Späth, F., Ingwersen, J., and Wulfmeyer, V.: Investigation of PBL schemes combining the WRF model simulations with scanning water vapor differential absorption lidar measurements, J. Geophys. Res.-Atmos., 121, 624–649, https://doi.org/10.1002/2015JD023927, 2016.

Molnár, G., Gyöngyösi, A. Z., and Gál, T.: Integration of an LCZ-based classification into WRF to assess the intra-urban temperature pattern under a heatwave period in Szeged, Hungary, Theor. Appl. Climatol., 138, 1139–1158, https://doi.org/10.1007/s00704-019-02881-1, 2019.

Nakayama, H., Takemi, T., and Nagai, H.: Large-eddy simulation of urban boundary-layer flows by generating turbulent inflows from mesoscale meteorological simulations, Atmos. Sci. Lett., 13, 180–186, https://doi.org/10.1002/asl.377, 2012.

Niu, G.-Y., Yang, Z.-L., Mitchell, K. E., Chen, F., Ek, M. B., Barlage, M., Kumar, A., Manning, K., Niyogi, D., Rosero, E., Tewari, M., and Xia, Y.: The community Noah land surface model with multiparameterization options (Noah-MP): 1. Model description and evaluation with local-scale measurements, J. Geophys. Res., 116, D12109, https://doi.org/10.1029/2010JD015139, 2011.

Panosetti, D., Böing, S., Schlemmer, L., and Schmidli, J.: Idealized Large-Eddy and Convection-Resolving Simulations of Moist Convection over Mountainous Terrain, J. Atmos. Sci., 73, 4021–4041, https://doi.org/10.1175/JAS-D-15-0341.1, 2016.

Pfister, G. G., Parrish, D. D., Worden, H., Emmons, L. K., Edwards, D. P., Wiedinmyer, C., Diskin, G. S., Huey, G., Oltmans, S. J., Thouret, V., Weinheimer, A., and Wisthaler, A.: Characterizing summertime chemical boundary conditions for airmasses entering the US West Coast, Atmos. Chem. Phys., 11, 1769–1790, https://doi.org/10.5194/acp-11-1769-2011, 2011.

Prein, A. F., Langhans, W., Fosser, G., Ferrone, A., Ban, N., Goergen, K., Keller, M., Tölle, M., Gutjahr, O., Feser, F., Brisson, E., Kollet, S., Schmidli, J., van Lipzig, N. P. M., and Leung, R.: A review on regional convection-permitting climate modeling: Demonstrations, prospects, and challenges, Rev. Geophys., 53, 323–361, https://doi.org/10.1002/2014RG000475, 2015.

Resler, J., Eben, K., Geletič, J., Krč, P., Rosecký, M., Sühring, M., Belda, M., Fuka, V., Halenka, T., Huszár, P., Karlický, J., Benešová, N., Ďoubalová, J., Honzáková, K., Keder, J., Nápravníková, Š., and Vlček, O.: Validation of the PALM model system 6.0 in real urban environment; case study of Prague-Dejvice, Czech Republic, Geosci. Model Dev. Discuss. [preprint], https://doi.org/10.5194/gmd-2020-175, in review, 2020.

Rieger, D., Bangert, M., Bischoff-Gauss, I., Förstner, J., Lundgren, K., Reinert, D., Schröter, J., Vogel, H., Zängl, G., Ruhnke, R., and Vogel, B.: ICON–ART 1.0 – a new online-coupled model system from the global to regional scale, Geosci. Model Dev., 8, 1659–1676, https://doi.org/10.5194/gmd-8-1659-2015, 2015.

Salamanca, F. and Martilli, A.: A new Building Energy Model coupled with an Urban Canopy Parameterization for urban climate simulations—part II. Validation with one dimension off-line simulations, Theor. Appl. Climatol., 99, 345–356, https://doi.org/10.1007/s00704-009-0143-8, 2010.

San José, R., Pérez, J. L., and González, R. M.: Very High Resolution Urban Simulations with WRF/UCM and CMAQ over European Cities, in: Urban Environment: Proceedings of the 11th Urban Environment Symposium (UES), held in Karlsruhe, Germany, 16–19 September 2012, edited by: Rauch, S., Morrison, G., Norra, S., and Schleicher, N., Springer Netherlands, Dordrecht, s.l., 293–301, https://doi.org/10.1007/978-94-007-7756-9_25, 2013.

Schell, B., Ackermann, I. J., Hass, H., Binkowski, F. S., and Ebel, A.: Modeling the formation of secondary organic aerosol within a comprehensive air quality model system, J. Geophys. Res., 106, 28275–28293, https://doi.org/10.1029/2001JD000384, 2001.

Scherer, D., Antretter, F., Bender, S., Cortekar, J., Emeis, S., Fehrenbach, U., Gross, G., Halbig, G., Hasse, J., Maronga, B., Raasch, S., and Scherber, K.: Urban Climate Under Change [UC]2 – A National Research Programme for Developing a Building-Resolving Atmospheric Model for Entire City Regions, Meteorol. Z., 28, 95–104, https://doi.org/10.1127/metz/2019/0913, 2019.

Schwitalla, T.: Simulation of NO_2 concentration over the Stuttgart metropolitan area, TIB AV-Portal, https://doi.org/10.5446/50923, 2021a.

Schwitalla, T.: Simulation of PM_{10} concentration over the Stuttgart metropolitan area, TIB AV-Portal, https://doi.org/10.5446/50924, 2021b.

Schwitalla, T., Warrach-Sagi, K., Wulfmeyer, V., and Resch, M.: Near-global-scale high-resolution seasonal simulations with WRF-Noah-MP v.3.8.1, Geosci. Model Dev., 13, 1959–1974, https://doi.org/10.5194/gmd-13-1959-2020, 2020.

Seidel, D. J., Zhang, Y., Beljaars, A., Golaz, J.-C., Jacobson, A. R., and Medeiros, B.: Climatology of the planetary boundary layer over the continental United States and Europe, J. Geophys. Res., 117, D17106, https://doi.org/10.1029/2012JD018143, 2012.

Skamarock, W. C., Klemp, J. B., Dudhia, J., Gill, D. O., Liu, Z., Berner, J., Wang, W., Powers, J. G., Duda, M. G., Barker, D. M., and Huang, X.-Y.: A Description of the Advanced Research WRF Model Version 4, NCAR, Boulder, CO, USA, 2019.

Steeneveld, G. J., Ronda, R. J., and Holtslag, A. A. M.: The Challenge of Forecasting the Onset and Development of Radiation Fog Using Mesoscale Atmospheric Models, Bound.-Lay. Meteorol., 154, 265–289, https://doi.org/10.1007/s10546-014-9973-8, 2015.

Stockwell, W. R., Middleton, P., Chang, J. S., and Tang, X.: The second generation regional acid deposition model chemical mechanism for regional air quality modeling, J. Geophys. Res., 95, 16343, https://doi.org/10.1029/JD095iD10p16343, 1990.

Stuttgart Municipality and German Meteorological Service (DWD): Requirements for fine dust situations, available at: https://feinstaubalarm.stuttgart.de/img/mdb/item/584405/119353.pdf last access: 20 August 2020, 2019.

Sun, W., Liu, Z., Chen, D., Zhao, P., and Chen, M.: Development and application of the WRFDA-Chem three-dimensional variational (3DVAR) system: aiming to improve air quality forecasting and diagnose model deficiencies, Atmos. Chem. Phys., 20, 9311–9329, https://doi.org/10.5194/acp-20-9311-2020, 2020.

Teixeira, J. C., Fallmann, J., Carvalho, A. C., and Rocha, A.: Surface to boundary layer coupling in the urban area of Lisbon comparing different urban canopy models in WRF, Urban Climate, 28, 100454, https://doi.org/10.1016/j.uclim.2019.100454, 2019.

Thompson, G., Field, P. R., Rasmussen, R. M., and Hall, W. D.: Explicit Forecasts of Winter Precipitation Using an Improved Bulk Microphysics Scheme. Part II: Implementation of a New Snow Parameterization, Mon. Weather Rev., 136, 5095–5115, https://doi.org/10.1175/2008MWR2387.1, 2008.

Thundathil, R., Schwitalla, T., Behrendt, A., Muppa, S. K., ADAM, S., and Wulfmeyer, V.: Assimilation of Lidar Water Vapour Mixing Ratio and Temperature Profiles into a Convection-Permitting Model, J. Meteorol. Soc. Jpn., 98, 959–986, https://doi.org/10.2151/jmsj.2020-049, 2020.

Thunis, P., Degraeuwe, B., Pisoni, E., Trombetti, M., Peduzzi, E., Belis, C. A., Wilson, J., and Vignati, E.: Urban $PM_{2.5}$ atlas: Air quality in European cities, JRC science for policy report, 28804, Publications Office, Luxembourg, 1 online resource, 2017.

UN: The World's Cities in 2018, United Nations, New York, USA, available at: https://www.un.org/en/events/citiesday/assets/pdf/the_worlds_cities_in_2018_data_booklet.pdf (last access: 23 March 2021), 2018.

Valcke, S., Balaji, V., Craig, A., DeLuca, C., Dunlap, R., Ford, R. W., Jacob, R., Larson, J., O'Kuinghttons, R., Riley, G. D., and Vertenstein, M.: Coupling technologies for Earth System Modelling, Geosci. Model Dev., 5, 1589–1596, https://doi.org/10.5194/gmd-5-1589-2012, 2012.

Vogel, B., Vogel, H., Bäumer, D., Bangert, M., Lundgren, K., Rinke, R., and Stanelle, T.: The comprehensive model system COSMO-ART – Radiative impact of aerosol on the state of the atmosphere on the regional scale, Atmos. Chem. Phys., 9, 8661–8680, https://doi.org/10.5194/acp-9-8661-2009, 2009.

Wang, D., Stachlewska, I. S., Song, X., Heese, B., and Nemuc, A.: Variability of the Boundary Layer Over an Urban Continental Site Based on 10 Years of Active Remote Sensing Observations in Warsaw, Remote Sensing-Basel, 12, 340, https://doi.org/10.3390/rs12020340, 2020.

Warrach-Sagi, K., Schwitalla, T., Wulfmeyer, V., and Bauer, H.-S.: Evaluation of a climate simulation in Europe based on the WRF–NOAH model system: precipitation in Germany, Clim. Dynam., 41, 755–774, https://doi.org/10.1007/s00382-013-1727-7, 2013.

WHO: WHO Air quality guidelines for particulate matter, ozone, nitrogen dioxide and sulfur dioxide, Global update 2005, Copenhagen, Denmark, available at: https://www.euro.who.int/__data/assets/pdf_file/0005/78638/E90038.pdf (last access: 23 March 2021), 2005.

WRF: The WRF-Chem code (version 4.0.3), available at: https://github.com/wrf-model/WRF/archive/v4.0.3.tar.gz, last access: 23 March 2021.

Yang, Z.-L., Niu, G.-Y., Mitchell, K. E., Chen, F., Ek, M. B., Barlage, M., Longuevergne, L., Manning, K., Niyogi, D., Tewari, M., and Xia, Y.: The community Noah land surface model with multiparameterization options (Noah-MP): 2. Evaluation over global river basins, J. Geophys. Res., 116, D12110, https://doi.org/10.1029/2010JD015140, 2011.

Zängl, G., Reinert, D., Rípodas, P., and Baldauf, M.: The ICON (ICOsahedral Non-hydrostatic) modelling framework of DWD and MPI-M: Description of the non-hydrostatic dynamical core, Q. J. Roy. Meteor. Soc., 141, 563–579, https://doi.org/10.1002/qj.2378, 2015.

Zhang, X., Huang, X.-Y., Liu, J., Poterjoy, J., Weng, Y., Zhang, F., and Wang, H.: Development of an Efficient Regional Four-Dimensional Variational Data Assimilation System for WRF, J. Atmos. Ocean. Techn., 31, 2777–2794, https://doi.org/10.1175/JTECH-D-13-00076.1, 2014.

Zhong, M., Saikawa, E., Liu, Y., Naik, V., Horowitz, L. W., Takigawa, M., Zhao, Y., Lin, N.-H., and Stone, E. A.: Air quality modeling with WRF-Chem v3.5 in East Asia: sensitivity to emissions and evaluation of simulated air quality, Geosci. Model Dev., 9, 1201–1218, https://doi.org/10.5194/gmd-9-1201-2016, 2016.

Zieliński, M., Fortuniak, K., Pawlak, W., and Siedlecki, M.: Long-term Turbulent Sensible-Heat-Flux Measurements with a Large-Aperture Scintillometer in the Centre of Łódź, Central Poland, Bound.-Lay. Meteorol., 167, 469–492, https://doi.org/10.1007/s10546-017-0331-5, 2018.